Accepted Manuscript

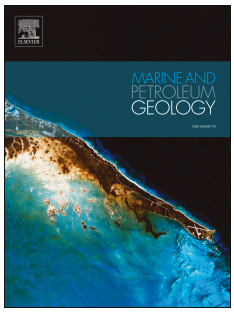

Exceptional reservoir quality in HPHT reservoir settings: examples from the Skagerrak Formation of the Heron Cluster, UK, North Sea

Stephan Stricker, Stuart J. Jones, Shanvas Sathar, Leon Bowen, Norman Oxtoby

PII: S0264-8172(16)30026-5

DOI: 10.1016/j.marpetgeo.2016.02.003

Reference: JMPG 2456

To appear in: *Marine and Petroleum Geology*

Received Date: 19 August 2015

Revised Date: 22 January 2016

Accepted Date: 2 February 2016

Please cite this article as: Stricker, S., Jones, S.J., Sathar, S., Bowen, L., Oxtoby, N., Exceptional reservoir quality in HPHT reservoir settings: examples from the Skagerrak Formation of the Heron Cluster, UK, North Sea, *Marine and Petroleum Geology* (2016), doi: 10.1016/j.marpetgeo.2016.02.003.

Exceptional reservoir quality in HPHT reservoir settings: examples from the Skagerrak Formation of the Heron Cluster, UK, North Sea.

Stephan Stricker[1*], Stuart J. Jones[1], Shanvas Sathar[1],Leon Bowen[2] and Norman Oxtoby[3]

[1]Department of Earth Sciences, Durham University, South Road, Durham, DH1 3LE, UK

[2]Department of Physics, Durham University, South Road, Durham, DH1 3LE, UK

[3]Fi[a] 41 Oaken Lane, Claygate, Surrey, KT10 0RG, UK

Abstract

As the exploration of hydrocarbons moves into more complex and deeper basinal settings the need to understand the effect of high temperatures and high pressures on reservoir quality and rock properties becomes even more important. The fluvial channel sandstone reservoirs of the Skagerrak Formation in the Central North Sea exhibit anomalously high porosities and permeabilities considering their depth of burial (> 3500 m below sea floor). Despite the complex depositional setting, diagenetic history, high overpressure and temperatures encountered in the Skagerrak Formation, hydrocarbons are currently being produced. The Skagerrak Formation reservoirs used in this study have encountered overpressures of >40 MPa and temperatures up to ~185°C at present day maximum burial. To identify the role played by the high pressure and high temperature encountered in the reservoir sandstones a multidisciplinary approach involving petrographic, fluid inclusion, and burial history modelling studies has been adopted. Our interpretation of the results is that the generation of shallow overpressure in these fields limited mechanical compaction and also played an important role in minimizing pressure solution in the chemical compaction regime as evidenced by reduced quartz cementation. Fluid inclusions found in the quartz overgrowths indicate late-stage development with temperatures of formation in the range 130-170°C coincident with late-stage deeper burial. Hydrocarbon emplacement occurred after quartz cementation and has had little to no effect on porosity preservation. The formation of well-developed authigenic chlorite (>70% surface coating) and, to a lesser extent illite clay coats with burial had a positive effect on porosity preservation even though permeability was marginally reduced in the illite-rich sandstones. A schematic porosity and quartz cement evolution model has been developed which allows for pre-drill prediction of reservoir quality in the Heron Cluster and provide valuable insights for other complex high-pressure high-temperature reservoirs.

Introduction

The inclusion of reservoir quality in pre-drill assessments is of paramount importance as hydrocarbon companies explore deeper targets. Exploration in deeply buried, high-pressure-high-temperature (HPHT; >65MPa and >150°C) reservoirs depends on identifying reservoir sandstones with sufficient porosity and permeability, especially where the reservoir has been exposed to elevated temperatures (>100°C) by prolonged burial.

In normally pressured reservoirs, sediments compact mechanically during burial as the vertical effective stress increases, so that the porosity is reduced. Mechanical compaction in sandstones has been reported to be dominant to burial depths of ~2000 m below sea floor (>70-80°C) (Bjørlykke, 1999, 2014). Porosity loss in sandstones can be generally predicted to some degree of accuracy giving rise to regional porosity-depth or porosity-temperature curves for many hydrocarbon basins (e.g. Ehrenberg et al., 2008). However, occurrences of sandstone reservoirs with higher than expected porosity are commonly attributed to conditions that limit the degree of burial compaction and/or cementation, or to pre-existing cements and grain coatings (e.g. Bloch et al., 2002; Taylor et al., 2010; Nguyen et al., 2013; Taylor et al., 2015).

Models for porosity preservation in deeply buried HPHT sandstone reservoirs (>4000 m below sea floor) tend to be focused on how clay (commonly chlorite) and microquartz detrital grain coatings can inhibit macro-quartz cementation. There are many studies where deep reservoir porosity is linked to early diagenetic clay or microquartz grain coats (e.g. Pittman et al., 1992; Ehrenberg, 1993; Aase et al., 1996; Bloch et al., 2002; Ajdukiewicz and Lander, 2010; Ajdukiewicz and Larese, 2012; French et al., 2012; Worden et al., 2012). These studies have shown that quartz-rich sandstones with well-developed and continuous diagenetic clay or microquartz grain coats contain a much lower volume of macro-quartz cement than without such coatings (Ajdukiewicz and Lander, 2010).

Albeit controversial, early hydrocarbon emplacement into a reservoir may also play a crucial role in the preservation of porosity (Worden and Morad, 2000; Worden et al., 1998). Field-based (Marchand et al., 2002) and experimental (Sathar et al., 2012) studies have shown that quartz cementation is inhibited at high oil saturations. However, other studies (e.g Aase and Walderhaug, 2005; Molenaar et al., 2008; Saigal et al., 1992) have suggested that there is no correlation between hydrocarbon emplacement and porosity preservation.

Fluid overpressure, defined as the excess pore pressure above the hydrostatic pressure for a given depth, reduces the effective stress acting on intergranular contacts and inhibits mechanical and chemical compaction (Osborne and Swarbrick, 1999). The shallow onset of pore fluid overpressure has been noted to enhance porosity preservation, in the Skagerrak Formation of the Central North Sea (Nguyen et al., 2013; Grant et al., 2014; Stricker and Jones 2016).

In this study we investigate the effect of HPHT reservoir conditions on sandstone porosity and permeability evolution in three deeply buried, siliciclastic reservoirs (Egret, Heron and Skua) from the Skagerrak Formation in the Heron Cluster (Egret, Heron and Skua, UK Quadrant 22), Central Graben, North Sea. Pore pressures exceed 80 MPa in the reservoir sandstones at present-day depths of 4000-5000 m below sea floor where temperatures are around 170-180°C (Table 1). A multidisciplinary approach comprising petrographic, SEM, fluid inclusion, and burial history modelling studies has been adopted in the present study to understand the evolution of reservoir quality in HPHT environments, with an explicit focus:

- How does the vertical effective stress history influence the porosity evolution of reservoir sandstones?
- How do authigenic grain coatings control quartz cementation and reservoir quality in the HPHT settings?

Geological setting

The Central Graben of the North Sea is a prolific hydrocarbon province containing more than 20 billion barrels of discovered hydrocarbons. The Central Graben is 70-130 km wide with an approximate length of 550 km. It is the southern arm of a trilete rift system (i.e., an incipient ridge-ridge triple junction) in the North Sea with the Viking Graben as the northern arm and the Moray Firth Basin as the western arm. The Central Graben is divided into the West and East sections by the Forties-Montrose and Josephine Ridge horst blocks (Fig. 1) and is flanked by the Norwegian basement in the East and the UK continental shelf in the West. The rift system developed in at least two major extension phases, one Permian-Triassic (290-210 Ma) and a Late Jurassic one (155-140 Ma) (Gowers and Sæbøe, 1985; Glennie, 1998). The geological history of the Central Graben is commonly divided into pre-rift, syn-rift and post-rift phases. The syn-rift sediments are the mainly siliciclastic Triassic and Jurassic sediments with approximately 2000m thickness. The post-rift sediments from the Cretaceous to the Holocene are as much as 4500m in thickness and dominated by shale, sandstones, silty sandstones and a thick chalk section (Glennie, 1998).

The focus of this study is on the HPHT sections at the southern end of the Forties-Montrose High in the UK quadrant 22 (Fig. 1). Cores of Skagerrak Formation reservoirs from three fields Skua, Egret, and Heron fields were utilized in this study (Fig. 1) The area is a part of a wider HPHT province, including the Triassic strata of the Central Graben and the southern Viking Graben (Goldsmith et al., 2003).

Triassic Skagerrak Formation Stratigraphy

The Triassic strata of the Central North Sea area are dominated by thick alluvial successions with no connection to a marine realm (Goldsmith et al., 2003). The Middle to Late Triassic Skagerrak Formation comprises deposits of 500-1000 m of predominantly continental braided and meandering fluvial systems and terminal fluvial fans with lacustrine facies in the Central

Graben, North Sea (McKie and Audretsch, 2005; De Jong et al., 2006; Kape et al., 2010). The stratigraphic nomenclature of the Triassic for the Central Graben was defined by Goldsmith et al. (1995, 2003), based on detailed biostratigraphic and lithostratigraphic correlation of wells from the Josephine ridge and was extended and correlated towards the ETAP (Eastern Trough Area Project) area by Mckie and Audretsch (2005). The Central Graben Triassic succession is subdivided into the Early Triassic Smith Bank Formation (shales, evaporites and thin sands) and the Middle to Late Skagerrak Formation (thickly interbedded sands and shales) (Fig. 2). The Skagerrak Formation is subdivided into three sand-dominated successions (Judy, Joanne and Josephine) and three mud-dominated successions (Julius, Jonathan and Joshua) (Fig. 2). The sand-dominated units include sheetflood deposits and multi-storey stacked channel sandbodies (Goldsmith et al., 1995; McKie and Audretsch, 2005), whereas the mud-dominated units include a variation of non-marine, basin wide floodplain and playa lake deposits. The thick and laterally extensive mud-dominated units provide the main correlative units for the Skagerrak in the Central Graben (McKie and Audretsch, 2005). The resultant Triassic stratigraphy in the Central Graben is incompletely preserved due to deep erosion during the Middle and Late Jurassic (Erratt et al., 1999).

The Triassic Smith Bank and Skagerrak sediments accumulated directly on top of the thickly developed Late Permian Zechstein salt in a series of salt and fault controlled mini-basins or pods. The Late Permian Zechstein salt controlled strongly the deposition by forming salt withdrawal mini basins due to a combination of localised loading and structural extension (Smith et al., 1993; Bishop, 1996; Matthews et al., 2007) within an overall rift controlled basin. The Smith Bank sediments represent the bulk and basal part of the pod infill, whereas the overlying Skagerrak is found as intra-pod sediments in the upper parts of the pods and as inter-pod sediments between the pods. The pod development was active throughout the

Triassic and mainly was responsible for the preservation of Middle to Late Skagerrak Formation in the study area. The thick Late Permian evaporite sediments (>2km) prevented grounding of pods on the underlying Rotliegend basement in the Central Graben. The salt tectonics created variable thicknesses between intra- and inter-pod Skagerrak sediments and allowed thick accumulations within the pods. Furthermore the salt pods created facies variability between intra- and inter-pods that influenced reservoir thickness and diagenetic cementation (e.g. Nguyen et al., 2013).

The Skagerrak stratigraphy in the study area consists of the Judy Sandstone Member, and is bounded by regional shale markers of the Marnock and Heron Shales, representing an equivalent to the Julius mudstone member and the upper Smith Bank Formation (Fig. 2; McKie and Audretsch, 2005). The Judy Member is also further subdivided by McKie & Audretsch (2005) into a lower terminal splay dominated interval and an upper channelised interval, separated by a shale prone section. The lower terminal splay facies is characterized by fine-grained, planar cross-bedded and ripple-laminated sandstones. In comparison, the upper interval is dominated by channel-fill deposits, which are organized into fining upward packages with coarse lag deposits (usually with ripped-up calcrete nodules) commonly occurring at the base. Channel-fill deposits are characterized by well sorted cross-bedded sandstones and can be separated in channel and sheet-dominated sandstones (McKie and Audretsch, 2005; McKie, 2011).

Methodology

Sampling

Core samples and thin sections examined in this study are from the Skagerrak Formation reservoirs from three fields, Egret (well 22/24d-10), Heron (well 22/29-5RE) and Skua (well 22/24b-7). A total of 274 core samples have been taken, from the Egret field (106) (22/24d-10) at depths between 4350 to 4570 m TVDSS (true vertical depth minus elevation above

mean sea level), from the Heron field (136) (22/29-5) at depths between 4300 to 4500 m TVDSS, and from the Skua field (32) (22/24b-7) from 3600 to 3660 m TVDSS. The depth intervals have been chosen to cover the main reservoir unit, the Judy Sandstone Member and the samples have been selected on a best expected reservoir quality strategy from the available core material. The focus on best reservoir quality has restricted the facies used in this study to confined, channelised and unconfined, sheetflood and crevasse splay components of the Skagerrak fluvial system (N. Meadows, 2015, *personal communication*). The Skagerrak sandstone reservoirs are currently at maximum burial depth and experience maximum temperatures and formation pressures (Table 1).

Petrography

Core sample thin sections were used to measure optical porosity, grain size and fraction of clay-coated grains for this study. Optical porosity was measured by using the digital image analysis technique, jPOR (Grove and Jerram, 2011), on blue epoxy-impregnated thin sections. Grain size distribution was analysed by using the Leica QWin (V. 3.5.0) software on thin section micrographs and the fraction of chlorite-coated grains were measured by point counting with 300 counts per thin section. Furthermore, additional petrographic analysis (i.e. intergranular volume (IGV) (Paxton et al., 2002), total cement volume (C)) were undertaken and measured by point counting with 300 counts per thin section using a standard petrographic microscope.

Thin sections from all three fields were highly polished to 30μm and coated with carbon prior to analysis by a Hitachi SU-70 field emission gun scanning electron microscope (SEM) and equipped with an energy-dispersive detector (EDS). Scanning electron microscope analyses of thin section and bulk rock samples were conducted at 5 to 20kV acceleration voltage with beam currents of 1 and 0.6nA, respectively. Point analyses had an average duration of 2 minutes, whereas line analyses were dependent on length. SEM-EDS was used

for rapid identification of chemical species (i.e. chlorite Fe/Mg ratio) and orientation on the sample. Cathodoluminescence analysis has been undertaken on selected thin sections with visible macro-quartz overgrowths using a Gata MonoCL system with a panchromatic imaging mode operated at 8 kV.

Fluid inclusion analysis

Microthermometry was conducted on double polished detached wafers to determine the conditions of cementation and evidence for formation water salinity. Fragments were cut from doubly polished rock wafers. The wafers were firstly checked under incident UV on a petrographic microscope to determine which contain petroleum inclusions and under transmitted light to determine the distribution of both aqueous and non-aqueous fluid inclusions for subsequent analyses. A Linkam THM600/TS90 heating – cooling stage connected to a Nikon petrographic microscope was used to obtain temperature data. Instrumental precision is +/- 0.1°C, while accuracy, dependent on the manufacturer's stated accuracy for the calibration standards used (synthetic inclusions and pure organic compounds) is better than +/- 0.1°C, over the range of temperatures reported here. Routinely available measurements are homogenization temperatures (T_h) and final melting temperatures (T_m). Homogenization is the conversion of multiphase inclusion contents to a single phase (usually at temperatures above room temperature). Interpreting homogenization temperatures in carbonates, sulphates and halides can be complicated because aqueous inclusions can (though not necessarily do) reset to higher temperature if they are a) overheated beyond a threshold which is dependent on the mineral strength and inclusion geometry (Goldstein and Reynolds, 1994), or b) frozen. This can occur in the laboratory as well as through geological processes, so care is taken in the order in which analyses are made for each rock chip. If resetting has occurred, larger inclusions may give higher temperatures, homogenization temperature distributions may show a high temperature tail and data from paragenetically

distinct settings may overlap. Final melting occurs at the disappearance of the last trace of solid in the inclusion on heating (usually after cooling an inclusion to well below room temperature). If ice is the final phase to melt (as in the present study) salinities are calculated using the equation given by Oakes et al., 1990.

One dimensional basin modelling

One-dimensional basin modelling provides an insight into the burial history of a reservoir and especially the temperature and pore fluid pressure evolution of the reservoir. Pore pressure built up by disequilibrium compaction and pore fluid volume expansion can be modelled with one-dimensional basin models such as the burial history simulation software PetroMod. Schlumberger's burial history simulation software PetroMod (V. 2012.2) was used in this study to model the temperature and pore pressure evolution of the Egret, Heron, and Skua fields. One-dimensional models are generally well suited to model pore pressure mechanisms such as disequilibrium compaction and pore fluid expansion but are limited in terms of integrating mechanisms such as lateral fluid flow or hydrocarbon charging. PetroMod is based on a forward modelling approach to calculate the geological evolution of a basin and burial history. Present-day well stratigraphy, well log lithology and lithological description were used to set the one-dimensional burial models (Fig. 2 & Table 2). Palaeo-basement heat flow was assumed according to Allen and Allen (1990) with 63 to 110 mW/m^2 (average of 80 mW/m^2) during syn-rift phases and 37 to 66 mW/m^2 (average 50mW/m^2) during post-rift phases. The burial history models are calibrated against present-day RFT temperature measurements corrected after Andrews-Speed et al. (1984), measured Skagerrak Formation porosities (Fig. 3) and carefully adjusted towards present-day formation pressure measurments by considering late stage, high temperature overpressure mechanisms (Osborne and Swarbrick, 1997; Isaksen, 2004). Vitrinite reflectance data, maximum temperatures obtained from apatite fission-track analyses, palaeotemperatures and palaeopore pressures

obtained from fluid inclusions in mineral cements were used to help calibrate the model (Swarbrick et al., 2000; di Primio and Neumann, 2008). We also conducted new fluid inclusion analysis in quartz cements to further constrain palaeotemperatures. The lithological unit types used in the models are PetroMod default lithology types or mixed default lithology types, chosen on the basis of well log descriptions and core analysis reports. Exceptions are the Hod lithology type and the lithology type of the Triassic Skagerrak sandstone members. The Hod chalk unit is modified to represent the North Sea non-reservoir chalk and match the compaction trend and permeability trend given by Mallon and Swarbrick (2002, 2008) (Table 3). The Triassic Skagerrak sandstone of the Judy Sandstone Members is simulated by a mix of PetroMod (V. 2012.2) default lithologies (80% sand, 10% silt, 10% shale) in combination with a regional compaction trend for shaly sandstone given by Sclater and Christie (1980).

Petrography, burial modelling and diagenesis

The present-day reservoir quality of the deeply buried Skagerrak Formation in the Egret, Heron, and Skua fields is a cumulative product of depositional attributes (e.g. facies architecture, grain composition, sorting, and size), mechanical compaction and diagenesis during shallow and deep phases of burial.

Burial history modelling results

The one-dimensional burial history models are based on well data and are calibrated with measured RFT pore pressure data, measured and corrected RFT temperatures and aqueous fluid inclusion homogenization temperatures of the Judy Sandstone Member (Table 4). The burial history models show the Skagerrak Formation reservoir sandstones are at maximum burial depth and temperatures at present day (Table 1). The Skagerrak Formation experienced in general a long shallow burial phase (~150 Myr) followed by a phase of rapid burial starting between 90-70 Ma to their present maximum burial depth (Fig. 5). The phase of rapid burial

was accompanied by significant temperature and pore pressure increases to their present day maxima. The present-day pore fluid pressure profiles of the three wells increases through the Chalk units (Ekofisk, Tor and Hod Formations) from hydrostatic to highly overpressured in the Skagerrak Formation reservoir sandstones.

The Egret burial history model shows a burial rate increase from ~90 Ma onwards, leading to a present day maximum burial depth of ~4300 m below sea floor (Formation top). Modelled reservoir temperature and pore fluid overpressure increase constantly during the rapid burial phase to present day maxima of 180°C and 39 MPa, respectively (Fig. 5; Table 1). The rapid overpressure increase in the Skagerrak Formation induces a reduction of the vertical effective stress (VES) accrual, which led to a maximum VES of ~24 MPa at around 10Ma and a present day VES of 10.4 MPa.

The Judy Sandstone Member of the Heron field have undergone a shallow burial phase (<1150 m below sea floor) followed by rapid burial from 90 Ma onwards to their present day maximum depth of around ~4300 m below sea floor (Formation top; Fig. 5). The burial history model shows an increase of pore fluid overpressure from 60 Ma towards a maximum present day overpressure of 40 MPa which leads to a decrease of the VES in the Skagerrak sandstone reservoirs to a maximum VES of 21.5 MPa and a present day VES of 6 MPa (Fig. 5). The modelled temperature of the Judy Sandstone Member in the Heron field is below 50°C for the early shallow burial phase and starts to increase during the rapid burial phase to a present-day maximum of 178°C for the Judy Sandstone Member.

The Judy Member of the Skua reservoir is subjected to a phase of a rapid burial from around 70 Ma with an even further increased burial rate in the last 10 Myrs towards present day maximum burial depth of 3500 m below sea floor (Formation top) (Fig. 5). The phase of rapid burial is coupled with temperature and pore fluid overpressure increases, especially the last 10 Myrs, towards 152°C and 26.6 MPa at present-day (Fig. 5). The overpressure increase

with ongoing burial reduced the VES accrual significantly to a lower maximum VES of 21.5 MPa at ~10Ma and a present-day VES of 12 MPa.

Grain size, porosity and degree of compaction

The 274 investigated samples from the Egret, Heron and Skua fields show a wide porosity range from <1% up to a maximum of 34% (Fig. 3). The measured optical porosity data is complemented by helium core plug porosities (measured after Boyle's law, uncorrected for possible decompaction effect). The Skagerrak reservoir sandstones in this study cover a narrow range of compositions and are classified as arkosic to lithic-arkosic arenites.

The Egret field (well 22/24d-10) data set shows optical porosities from <1% to up to 14% porosity, with an average of 7% and helium core plug porosities from 10% to 31%, with a mean around 20% (Fig. 3). The grain sizes vary from coarse silt to medium-grained sand, with an average grain size of 0.136 mm and the majority of the samples between very fine and fine-grained sand (Fig. 4).

The Heron field (well 22/29-5RE) data set in comparison show a wider optical porosity range from <1% to up to 31%, with the majority of the porosity values below 15% and a mean of 6%. The helium core plug porosities are in general higher with a maximum of 29% and a mean of 20% (Fig. 3). The grain sizes vary from coarse silt to medium-grained sand, with a mean grain size of 0.136 mm and the majority between very fine and fine-grained sand (Fig. 4).

Porosity data from the Skua field (well 22/24b-7) samples show a wide range from <1% to 31% for the optically measured porosities and 3% to 27% for the helium porosities. The mean of optical and helium porosities is around 11% and 17%, respectively (Fig. 3). The grain sizes vary between very fine and fine-grained sand (Fig. 4), with an average grain size of 0.169 mm.

Interestingly, grain-size variability is limited across all facies, with most of the sandstones being fine and very fine grained with a grain size between 0.063 and 0.25mm (Fig. 4). Coarser grain sizes are encountered within the lower parts of the confined channelized sands, with a mean grain size of 0.35 mm (medium grain size).

The Egret, Heron, and Skua samples show features of mechanical compaction of soft grains, such as deformed lithic clay grains, kinked mica grains and minor chemical compaction features such as concavo-convex grain contacts at detrital quartz grain boundaries. However, the sample sets indicate under-compaction in relation to hydrostatically pressured sandstones at equivalent burial depth (porosity-depth relationship for hydrostatically pressured shaly sandstone by Sclater and Christie (1980)) to the present-day burial depth of the Judy Sandstone Member. The under-compaction of the Skagerrak sandstones is further highlighted by the general absence of strong chemical compaction features, such as sutured or stylolitic grain contacts.

Diagenetic cements and grain coatings

The complex diagenetic history of the Skagerrak Formation sandstone reservoirs has been described by a number of research papers (e.g. Smith et al., 1993; Weibel, 1998; Swarbrick et al., 2000; Kape et al., 2010; Nguyen et al., 2013). The main diagenetic cements recognised include quartz, localised carbonate (ferroan dolomite), feldspar, and early precipitates of halite cement as identified by (Nguyen et al., 2013). Detrital quartz grains were reported to be coated by clay minerals such as chlorite and more rarely illite in the Skagerrak Formation and their presence has been correlated to low quartz cement volumes (Taylor et al., 2010; Nguyen et al., 2013; Taylor et al., 2015). The major cement types and clay mineral coatings, important for reservoir quality in this study, are discussed in more detail below.

Carbonate cements

Carbonate cements are very localised throughout the Skagerrak Formation and sourced by syn-depositional calcitic palaeosols in very fine grained floodplain deposits or by calcrete and dolocrete rip-up clast at channel bases (McKie et al., 2010). The scarce carbonate cements in the three data sets are mainly present as deformed carbonate-clay rip-up clasts (Fig. 7A) or as pore filling cements often associated with "megapores" in channel base samples. The clay free carbonate cements show a rhombic crystal structure with a prominent cleavage pattern and tend to infill the pore space completely where they are present (Fig. 7B). Fluid inclusion analysis on carbonate cement in the Skua sample 2 shows high aqueous and lower non-aqueous fluid inclusions homogenization temperatures of 138°C to 144.5°C and 79°C to 112°C, respectively (Table 4).

Grain coatings

Grain coatings and especially authigenic clay minerals are common in all of the Skagerrak sandstones (e.g. Nguyen et al., 2013; Taylor et al., 2015). Detailed petrography, SEM and SEM-EDS analysis presented in this study has identified authigenic clay mineral grain coatings on detrital quartz grains; consisting of mainly authigenic chlorite in the Heron and the Skua fields (Fig. 8B & C) and a mixture of authigenic chlorite and illite in the Egret field (Fig. 8A). The authigenic clay coatings are fully transformed at present-day and no prove of precursor clay minerals has been detected. Grain coating chlorite is analysed using SEM-EDS and classified according to the Fe/Mg ratio (Hillier and Velde, 1992):

$$Fe/Mg\ ratio = \frac{Fe}{(Fe + Mg)} \qquad \textbf{(1)}$$

Chlorite coats are classified as intermediate to Fe-rich for the Egret and Heron samples, with Fe/Mg ratio of 0.4-0.55 (Egret) and 0.45-0.6 (Heron) and as intermediate to Mg-rich for Skua (0.35-0.5) (Table 5).

The majority of samples have measured grain coating values of more than 70% and several with near complete chlorite coatings (Fig. 9). The Heron and Skua data sets have high measured grain coating values of 79.2% and 70.1% respectively (Fig. 9). The grain coatings are in general continuously developed and range from 1μm to 20μm thick, with an average thickness of 11 μm. The chlorite coatings show a complex structural pattern, regardless of their thickness, with a dense root zone (Pittman et al. 1992) of laminated crystals oriented parallel to the detrital quartz grain surface (Fig. 8D). These are superseded by well-defined chlorite crystals growing normal to the root zone (Fig. 8B, C & D). In comparison, the Egret data set has a higher fraction of chlorite coated detrital quartz grains of 86.1% (Fig. 9). These chlorite coatings are better developed with an average thickness >15μm, but commonly coexist with illite on detrital quartz surfaces (Fig. 8A & E). Furthermore, these coating root zones have a more dense structure of amorphous to poorly defined chlorite and illite crystals (Fig. 8F) and are superseded by well-developed chlorite platelets and fibrous and flaky illite, which are in randomly orientation to each other, but normally oriented to the detrital grain surface (Fig. 8A, E & F). The observed coating structure,with a root zone and superseding crystals, has been described by several authors for authigenic clay mineral coatings (e.g. Pittman and Lumsden, 1968; Wilson and Pittman, 1977; Pittman et al., 1992; Ajdukiewicz and Larese, 2012; Haile et al., 2015).

The occurrence and importance of grain coating chlorite in the Skagerrak sandstone reservoirs has been reported from the J-ridge area (Nguyen et al., 2013; Grant et al., 2014) and the Heron Cluster (McKie et al., 2010; Taylor et al., 2015). However, the mixed chlorite-illite coatings of the Egret samples show a tendency to bridge between grain coatings and thereby fill the pore space and block pore throats. This is less common in the Heron and Skua sample sets where the overall clay mixture consists predominantly of chlorite and <5% illite. In general, pore-filling cements comprise smaller and less well developed chlorite crystals

within a denser packing arrangement than seen for the grain coatings. The optical porosity loss by pore filling clay cements can be up to 15% in some samples.

Quartz cements

Quartz cements can be recognised in all three sample sets in this study and two types of cement growth are recognised, either as very thin microquartz grain coatings (Fig. 7C, 8B & 11A) or as a more blocky and thick macro-quartz overgrowth, present at non-coated grain surfaces or at breaks within the chlorite coatings (Fig. 7C, 7D & 11B). The term microquartz overgrowth is here used for polycrystalline growth patterns of individual micro-sized quartz crystals ranging from 1 to 10μm in length, which are in optical continuity or discontinuity with the detrital quartz grain (Aase et al., 1996; French and Worden, 2013). In comparison macro-quartz overgrowth is defined as syntaxial quartz overgrowth larger than 20 μm in optical continuity with the detrital quartz grain. The amount of quartz cement in general is very low in the three investigated sample sets (<5% bulk volume), but can exceed 5% bulk volume in single samples.

Fluid inclusion analyses have been undertaken on selected samples with higher quantities of quartz overgrowths and show high homogenization temperature for the fluid inclusions. The aqueous homogenization temperatures range from 145°C to 171°C for the Egret sample, 104°C to 116°C and 133°C to 163°C for the Heron samples, and 133°C to 156°C for the Skua samples (Table 4). The non-aqueous fluid inclusions are generally less common in the sample sets. Homogenization temperatures are between 70°C to 77°C for the Heron sample 1 and are at 83°C for one inclusion in one of the Skua samples (Table 4).

The microquartz overgrowth tends to fill small cavities in the detrital quartz grain surface and to infill void spaces between the detrital quartz grain surface and the chlorite mineral coating (Fig. 7C, 7E & 12C). Single microquartz crystals (<5μm) can be found in between the chlorite platelets and the illite fibres (for Egret samples), which tend to outgrow the clay

mineral coatings (Fig. 8B & 12C). This sublayer of microquartz precipitation beneath and in-between chlorite grain coatings has previously been recognized in high-temperature experimental studies by Ajdukiewicz and Larese (2012).

K-Feldspar dissolution & cementation

K-feldspar dissolution and alteration can be observed in each of the sample sets. K-feldspar dissolution occurs generally during late burial stage, indicated by clay mineral coatings, which preserve the original K-feldspar grain shape of partly or fully dissolved grains. The volume of K-feldspar cement ranges from approximately <1% to a maximum of 5%. Minor amounts of late stage blocky authigenic K-feldspar overgrowth can be observed on uncoated and partly dissolved K-feldspar grains. Aqueous fluid inclusions in feldspar overgrowths in the Egret sample indicate cementation at high temperatures above 140°C. Non-aqueous fluid inclusions encountered in feldspars show significantly lower temperatures between 45°C and 118°C across the three sample sets (Table 4). Highly altered and dissolved K-feldspar grains can coexist in close proximity to unaltered grains. Variations in feldspar microtextures exertis control on reactivity as demonstart5ed by Parsons et al. (2005).

Paragenetic sequence

The diagenetic development of the Skagerrak Formation in the investigated reservoirs is similar and therefore can be linked into a general relative sequence by their observed petrographic features (Fig. 6 & 7).

Evidence of mechanical compaction throughout the whole burial process is present in Egret, Heron and Skua sample sets and despite the overall shallow overpressure initiation and associated VES reduction mechanical compaction is still the main driver of porosity reduction during the first 2500 m of burial (Fig. 5). Nevertheless, the reduced VES accrual limited the effect of mechanical compaction significantly in the Skagerrak sandstones.

Therefore, mechanical compaction is lower than in equivalent hydrostatically pressured sandstones (represented by the porosity-depth relationship for hydrostatically pressured shaly sandstone by Sclater and Christie (1980) at equivalent depth (Fig. 3).

Diagenesis started at shallow burial with localised carbonate cementation (ferroan dolomite), mainly internally sourced by dissolution of reworked calcrete or dolocrete fragments (Fig. 7A; McKie and Audretsch, 2005). Shallow carbonate precipitation is indicated by high IGVs, close to the assumed initial sandstone porosity of 45%, in the cemented channel base samples. High fluid inclusion homogenization temperatures in the Skua sample set and large single crystals indicate further diagenetic changes at higher temperatures (Table 4 & Fig. 7B).

Authigenic clay mineral coatings developed after shallow carbonate cementation and prior to major quartz cementation (Fig. 7C & D). SEM and SEM-EDS analysis identified chlorite as the main coating clay mineral, alongside with a minor amounts illite.

Feldspar dissolution occurs after the beginning but generally alongside continuous precipitation of authigenic chlorite and illite clay minerals, which is indicated by clay mineral coated feldspar grains where chlorite and illite tend to infill and overgrow dissolution cavities of partly dissolved feldspars (Fig. 7F)

Fluid inclusions from blocky quartz overgrowth indicated late occurrence of quartz cementation at high temperatures of ~130-170°C in the Skagerrak Formation. Quartz cement can be recognised as either very thin microquartz grain coatings (e.g. Fig. 7C, 8B & 11A) or blocky and thick macro-quartz overgrowth, present at non-coated grain surfaces or at breaks within chlorite coatings (e.g. Fig. 7C, 7D & 11B). Several precipitation events can be observed for microquartz, indicated by various growth stages in cathodoluminescence images (Fig. 10A & C). High homogenization temperatures of up to 170°C for aqueous fluid

inclusions in blocky macroquartz overgrowth indicate very late quartz cementation in the Judy sandstone Member (Fig. 6).

The non-aqueous fluid inclusions suggest that hydrocarbon emplacement occurred late in the burial history of the Egret, Heron and Skua fields. The microthermometry results from the coexisting hydrocarbon and aqueous inclusions reveales a temperature of ~60-120°C for hydrocarbon inclusions and ~130-170°C for aqueous fluid inclusions (Table 4). However, the homogenization temperature for the aqueous inclusions (i.e. 130-170°C) represents the trapping temperature for both fluids as the oil was undersaturated with gas for the trapping pressure and temperature (Munz et al., 1999; Munz, 2001). The fluid inclusion results concur with the commencement of hydrocarbon generation from the end of the Cretaceous and was completed by mid-Miocene times (Lines and Auld, 2004).

Furthermore, feldspathic cementation can be observed and is identified as late stage cement by aqueous fluid inclusion homogenization temperatures (Table 4).

Porosity loss by mechanical compaction vs. cementation

Additional petrographic data such as intergranular volume (IGV) (Paxton et al., 2002) and total cement volume (C) can be used to calculate the porosity loss due to mechanical compaction (COPL) and cementation (CEPL) after Lundegard (1992):

$$COPL = P_i - \left(\frac{(100 - P_i) P_{mc}}{100 - P_{mc}} \right) \quad \textbf{(2)}$$

$$CEPL = (P_i - COPL)\left(\frac{C}{P_{mc}} \right) \quad \textbf{(3)}$$

where P_i is the initial or depositional porosity (here assumed with 45%; Beard and Weyl, 1973) and P_{mc} is the intergranular volume or minus-cement porosity calculated by subtracting the total cement volume (C) from the optical primary porosity. The calculated COPL and CEPL are only accurate if three conditions are met. First, the assumed initial porosity P_i is

correct. Second, the amount of cement derived by local grain dissolution is negligible or known. And third, the amount of framework mass exported by grain dissolution is negligible or known (Lundegard, 1992). The calculated porosity losses by mechanical compaction (COPL) and by cementation (CEPL) show a similar pattern for Egret, Heron and Skua fields (Fig. 11). The Average values of COPL and CEPL are 26.8% and 9.2%, with 29.1% and 8.8% for Egret, 24.8% and 9.6% for Heron and 26.4% and 9.1 % for Skua sample sets. This identifies that the main porosity loss in the Egret, Heron and Skua is mainly due to mechanical compaction rather than cementation (Fig. 11).

Discussion

Vertical effective stress and porosity evolution

The positive effect of pore fluid pressure and low VES on porosity preservation is well known since Therzagie's effective stress concept and therefore overpressured reservoirs are often associated with good reservoir quality. However, a combination of magnitude and timing of onset of overpressure needs to be considered for enhanced porosity preservation in siliciclastic reservoirs. Pore fluid overpressure can slow down or arrest mechanical compaction by reducing the vertical effective stress during ongoing burial, but cannot increase porosity. Therefore, overpressure developed during (shallow) initial burial is crucial for maintaining primary porosity and good reservoir quality to depth (e.g. Ramm and Bjørlykke, 1994; Osborne and Swarbrick, 1999; Schneider and Hay, 2001). Furthermore, overpressured reservoirs have no fluid exchange (i.e. fluid influx) with less overpressured areas, which allows them to evolve within their very own fluids (Jeans, 1994). This reduces the overall number of diagenetic processes that may affect the overall reservoir quality.

The pore fluid overpressure in the Skagerrak sandstone reservoirs initiate (0.01 MPa) at around 60 Ma (Egret & Heron) and 50 Ma (Skua) at shallow burial and increases with

ongoing burial to the present-day maximum. The very shallow onset and rapid increase of overpressure enabled the pore fluids to reduce the load borne by intergranular and cement-grain contacts within the sandstones (Fig. 12). It is to be noted that late development and deeper onset of overpressure would have had a much smaller to negligible effect on porosity preservation in the reservoir sandstones. The reduced stress on the grain framework causes a reduction in mechanical compaction and chemical compaction (pressure dissolution) at grain contacts (Osborne and Swarbrick, 1999). The reduced mechanical compaction rate can be easily observed in the datasets, where a predominance of point, long or concavo-convex grain contacts occurs compared to sutured or stylolitic quartz grain contacts which would be expected in deeply buried hydrostatic reservoirs. The effect of overpressure on reservoir quality is the highest with initiation depths above 1500m because at this depth range porosity or intergranular volume reduction in hydrostatic pressured sandstones is particularly strong (from 42% to 28% on average, Paxton et al., 2002). Nevertheless, low VES can still have an impact on compaction processes beyond 1500m burial depth due to the lower limit of physical grain compaction of approximately 26% porosity or IGV at 2500m (Paxton et al., 2002), and late stage chemical compaction.

Significant porosity preservation is commonly suggested to occur during later stage chemical compaction due to of the occurrence authigenic chlorite grain coatings (e.g. Bloch et al., 2002; Ajdukiewicz and Larese, 2012; this study). However, it has been recognized that the rate of quartz cementation increases as an exponential function of temperature during burial and estimated that the rate may increase by a factor of 1.7 for every 10^{o}C temperature increase (Walderhaug, 1996). Temperature has been considered by far the most important control on the rate of quartz precipitation in deeply buried sandstones (Walderhaug, 1996; Bjorkum, 1996; Lander et al., 2008). The amount of quartz cementation and porosity can be modeled as an exponential function (Arrhenius equation) of the temperature integrated over

time and forms the basis of many commercially available reservoir quality predictive programs. The occurrence of minerals at grain contacts are also thought to be important and dissolution is considered to be enhanced by mica or clay minerals at quartz grain contacts (Bjorkum, 1996).

This study has provided evidence from the Skagerrak Formation sandstones that shallow onset of pore fluid pressure can arrest the rate of quartz cementation and maintain an enhanced porosity to greater burial depths than normally would be expected under hydrostatic conditions and as a function of temperature alone (Fig. 12). Quartz cementation is far more sensitive to pore fluid overpressure than has previous been attributed. This in part is due to the significant role low VES plays in limiting and forestalling the onset of intergranular pressure solution at grain contacts (e.g. Osborne and Swarbrick, 1999; Swarbrick et al., 2000; Sheldon et al., 2003; Becker et al., 2010 Stricker and Jones 2016). Quartz cementation and especially quartz overgrowths on detrital quartz grains are a widely reported diagenetic and porosity reducing processes in deeply buried quartz rich sandstones (e.g. McBride, 1989; Walderhaug, 1990; Vagle et al., 1994; Walderhaug, 1994b; Worden and Morad, 2000). Stylolitisation and dissolution at intergranular grain contacts is often reported as main internal source of quartz cement in many siliciclastic reservoirs (e.g. Houseknecht, 1988; Bjorkum et al., 1993; Walderhaug, 1994a, b). The low VES halted stylolitisation in the Skagerrak Formation sandstones and reduced stress on the grain framework and grain contacts (Fig. 12). The supply of dissolved silica towards the pore fluid is thereby reduced which leads to a lower silica saturation of the pore fluid and finally to lower and later quartz cement precipitation (Osborne and Swarbrick, 1999; Stricker and Jones, 2016).

Authigenic clay coatings and reservoir quality

The development of clay mineral coatings is often reported to be closely linked to the absence of extensive quartz cementation. The role played by clay mineral coatings in siliciclastic reservoirs is of significant interest for the maintenance of exceptional reservoir quality (e.g. Taylor et al., 2010; Ajdukiewicz and Larese, 2012).

Clay mineral coatings in the Skagerrak Formation are generally well-developed and consist mainly of authigenic chlorite, with minor amounts of authigenic illite (especially in the Egret field). SEM-EDS analysis of the chlorite coatings classify them as intermediate to Fe-rich for the Egret and Heron samples, with Fe/Mg ratio of 0.4-0.55 (Egret) and 0.45-0.6 (Heron) and as intermediate to Mg-rich for Skua (0.35-0.5) (Table 5) (Hillier and Velde, 1992). The observed Fe/Mg ratios correlate well with reported ratios between 0.25–0.65 for terrestrial sediments (Downey et al., 2011). The SEM-EDS analysis also showed that the authigenic chlorite and illite is fully transformed without any remnant precursor clay composition. Downey et al. (2011) reported three possible building mechanisms for chlorite grain coatings in fluvial environments; firstly grain coating Fe-rich clay minerals, secondly the mechanical infiltration of precursor clay minerals (e.g. smectite) and, thirdly the alteration of detrital grains. The chloritization and illitization of smectite is the most likely diagenetic pathway for authigenic chlorite and illite grain coatings in the Skagerrak formation. Mechanical infiltrated smectite has been probably attached flatly to the detrital grains during or shortly after deposition (Matlack et al., 1989) (Fig. 12). The chloritization of smectite requires a source of aluminum (e.g. Hillier, 1994; Humphreys et al. 1994) and takes place at temperatures between 60-100°C (e.g. Worden and Morad, 2003). Illitization of smectite also requires a source of aluminum and potassium and is reported to occur at temperatures above 90°C (e.g. Worden and Morad, 2003). Detrital smectite coatings have been continuously transformed into authigenic chlorite with increasing temperatures and dissolution of detrital k-feldspar (Fig. 7F & 12).

The authigenic chlorite grain coatings in the Heron Cluster fields are well-developed and cover more than 70% of the detrital grain surfaces (Fig. 9 & 12). Nevertheless, there are differences in composition and appearance. The coatings in the Heron and Skua sample sets are typical edge to edge chlorite coatings with a platy crystal structure similar to those observed by Pittman et al. (1992). The clay mineral coatings in the Egret field are generally thicker and contain a higher amount of fibrous illite (Fig. 8A & F). The Egret field coatings are structurally more variable in their morphology, compared with the Heron and Skua coatings. The general coating structure, described by Pittman et al. (1992), is consistent in all three sample sets, with a flatly attached root zone and superseding chlorite and/or illite crystals (Fig. 8 D). Where high amounts fibrous illite occur, the root zone is structurally less well developed and amorphous in comparison with a pure chlorite grain coatings (Fig. 8F)

Ajdukiewicz and Larese (2012) observed quartz nucleation below the root zone and in-between the crystals of the chlorite coatings at temperatures above 115°C and concluded that chlorite coatings may retard quartz nucleation at moderate temperatures, but permit quartz nucleation at high temperatures similar to those encountered in the Skagerrak Formation. This quartz tends to infill the microporosity of the chlorite coatings and produces a sub-layer beneath chlorite coatings. Intact chlorite coatings provide an effective barrier for potential quartz crystal growth from the detrital surface into the pore space, due to the high crystal interconnection (Pittman et al., 1992; Ajdukiewicz and Larese, 2012; Haile et al., 2015). Illite coatings on the other hand are in respect to chlorite coatings less able to prevent quartz outgrowth due to the normally oriented, fibrous crystals and the low degree of crystal interconnection (Guven et al., 1980; Storvoll et al., 2002; Wilson et al., 2014). The mixed clay coatings in the Egret field have a very high surface coverage (>85%; Fig. 9).

High homogenization temperatures for the aqueous fluid inclusions in the quartz overgrowth (Table 4; 145°C to 171°C) indicate the importance of clay mineral coatings and

vertical effective stress for retardation of quartz precipitation (Fig. 12). Mixed chlorite/illite coatings (Fig. 8F) provide a more effective barrier to quartz nucleation than chlorite coatings alone.

Microquartz grain coatings

Microquartz grain coatings are polycrystalline growth patterns of individual micro-sized quartz crystals ranging from 1 to 10μm in length, which are in optical continuity or discontinuity with the detrital quartz grain (Aase et al., 1996; French and Worden, 2013) and often reported to be closely linked to the absence of extensive macroquartz cementation. Microquartz coatings have been described as a layer of random oriented, micro-sized quartz crystals crystallographiclly misoriented with respect to the host grain (e.g. French et al., 2012; French and Worden, 2013). Microquartz can be observed in several appearances in the Skagerrak sandstones, such as a coating layer below clay coatings (Fig 7C & E) or as single crystals, outgrowing clay mineral coatings (Fig. 8B). Cathodoluminescence analysis of the microquartz in the three sample sets indicated multiple precipitation and growth events (Fig. 10A & C) mainly below the chlorite grain coatings and in between the chlorite crystals (Fig. 7E, 8E, 10C & 8B). The microquartz is likely to be precipitated at higher temperatures (>115°C) as demonstrated by Ajdukiewicz and Larese (2012).

However, the contribution of the microquartz coatings towards the preservation of reservoir quality is minor to negligible in the Skagerrak Formation. The presence of well-developed chlorite grain coatings and high pore fluid pressures have played a more significant role to inhibit extensive macroquartz cementation.

Macroquartz cementation and reservoir quality

Quartz cementation is generally scarce in the Skagerrak Formation but can be observed as micro and macro quartz cement at non-coated detrital grain surfaces in all three sample sets.

Quartz cementation starts generally at temperatures around 70-80°C (e.g. McBride, 1989; Walderhaug, 1994b, a; Worden and Morad, 2000) with very slow precipitation rates, which increase with increasing temperatures (Walderhaug, 1994b). Walderhaug (1994b) expressed the temperature dependence of macroquartz precipitation *r* mathematically:

$$r = 1.98 * 10^{-22} * 10^{0.022*T} \quad (4)$$

where *r* is precipitation rate in moles per square centimetre and *T* is temperature in degree Celsius. The quartz precipitation rate can be converted into a linear outwards growth rate for quartz cement in cm/s by multiplying r by the molar mass of quartz (60.08g/mol) and dividing by the density of quartz (2.65g/cm^3). This leads to linear quartz cement outgrowth rates as a function of temperature, e.g. 0.04908µm/Ma at 70°C or 1.70210µm/Ma at 140°C (Table 6). The calculated linear quartz growth rates can be used to estimate time necessary to enclose a small fluid inclusion (4µm) at certain temperatures (Table 6).

The comparison of the quartz growth rates for overgrowth and the rapid burial rates for the Triassic Skagerrak shows that fluid inclusions are unlikely to form at temperatures below 100°C to 110°C due to the slow quartz growth rates (Table 6) and the rapid burial rates of the Skagerrak Formation (Fig. 5). The lowest aqueous homogenization temperatures from quartz cements are consistent with this observation (Heron; Table 4), but the majority of the aqueous homogenization temperatures are beyond 130°C.

However, we have already argued for potential inhabitation of quartz cementation by clay coatings, microquartz coatings and particularly overpressure, and suggest that the combined effect of all these processes produce predominantly high temperature quartz overgrowths.

Conclusions

1. The HPHT Skagerrak Formation sandstone reservoirs of the Egret, Heron and Skua fields (UK quadrant 22) have total enhanced porosities in the range of 18-35%, despite their depth of burial and elevated high temperatures.
2. Porosity in the Skagerrak Formation was preserved through a combination of shallow onset of pore fluid pressures reducing mechanical compaction and well developed chlorite and mixed chlorite/illite grain coatings inhibiting quartz cementation.
3. The shallow onset of high pore fluid pressure (at end of Cretaceous) and maintenance to present day contributed towards the inhibition of macroquartz overgrowths by reducing pressure solution at detrital quartz grain contacts.
4. Authigenic chlorite and mixed chlorite/illite coat most detrital quartz grain surfaces (>70% surface coating) and restricted the development of abundant pore-filling quartz cement despite elevated temperatures (up to ~180°C at present day). The abundance of quartz cement correlates well with grain coat coverage and shows no relationship to the presence of hydrocarbon pore fluids.
5. Burial history modeling using detailed fluid inclusion analyses and quantitative petrography of the Skagerrak Formation reservoir sandstones has revealed that macroquartz overgrowths have been inhibited up to very high burial temperatures (~185°C) by low vertical effective stress and well developed clay mineral coatings. The results indicate that the range of porosities preserved provide potential for exploration in the deeper (>5500 m below sea floor) and HPHT portions of the Central Graben, North Sea.

Acknowledgments

The research consortium GeoPOP sponsored by BG, BP, Chevron, ConocoPhillips, DONG Energy, E.ON, ENI, Petrobras, Petronas, Statoil, Total and Tullow Oil, at Durham University are thanked for funding this research. We acknowledge support from the BGS for access to core material from the Heron Cluster wells. The results presented have been improved through collaborative discussions with many colleagues including Neil Goulty, Andy Aplin, Jon Gluyas, Neil Grant, Jamie Middleton and Neil Meadows.

Figures:

Figure 1 - Map of the southern part of the UK quadrant 22 with important regional structural features indicated.

Figure 2 - Stratigraphy of the Heron Cluster fields: Egret (well 22/24d-10), Heron (well 22/29-5) and Skua (well 22/24b-7).

Figure 3 - Optical and helium porosities of the Heron Cluster sample sets with a regional Central North Sea porosity-depth relationship for hydrostatically pressured shaly sandstone (Sclater and Christie, 1980) and the modelled sandstone porosities (circles).

Figure 4 - Grain size distribution of the Egret, Heron and Skua sample sets, with average grain size (Av.).

Figure 5 - Modelled vertical effective stress (VES) evolution, overpressure (OP) evolution, temperature evolution and burial depth for the Triassic Judy sandstone member of the Egret, Heron and Skua fields, including aqueous quartz overgrowth fluid inclusion homogenization temperatures (FI QTZ OG).

Figure 6 – Paragenetic sequence of the main diagenetic processes for the Egret, Heron, and Skua fields, based on petrographic relationships and basin modelling, with fluid inclusion homogenization temperatures for aqueous carbonate, feldspar and quartz inclusions.

Figure 7 – Micrographs of A) calcrete/dolocrete fragments (Heron); B) a single dolomite crystal next to a deformed mica grain (Heron); C) a detrital quartz grain with macroquartz (blocky) and microquartz overgrowth (Skua); D) a detrital non-coated quartz grains with macroquartz overgrowth and fluid inclusions at the boundary between detrital grain and overgrowth (Heron); and SEM images of E) a detrital grain with chlorite coating and microquartz between the coating and the detrital grain (Heron); F) a partial dissolved feldspar with chlorite coating (Egret).

Figure 8 - SEM images of A) chlorite (chl) and illite mixed clay mineral coats (Egret); B) chlorite (chl) coatings with single outgrowing microquartz crystals (MQtz) (Heron); C) well developed authigenic chlorite (chl) grain coating (Skua); D) well developed authigenic chlorite (chl) coatings with a structured root zone (sRZ) (Skua); E) a detrital grain with microquartz overgrowth (MQtz) between mixed clay mineral coating (chl/illite) (Egret); F) amorphous root zone (aRZ) underlying illite grain coating (Egret).

Figure 9 - Fraction of clay coated detrital grains in Egret, Heron, and Skua sample sets, with the average of coated grains (Av.).

Figure 10 - SEM and CL images of A) microquartz growing on an detrital quartz grain (Egret); B) macroquartz overgrowth on an detrital quartz grain next to an clay mineral coated grain without quartz overgrowth (Egret); C) a fully chlorite coated grain with minor microquartz between the detrital grain and the chlorite coating (Skua).

Figure 11 - Compactional porosity loss (COPL) and cementational porosity loss (CEPL) for Egret, Skua, and Heron data sets, calculated according to Lundegard (1992).

Figure 12 – Schematic diagram for the comparison of A) a theoretical representation for a deeply buried siliciclastic reservoir of same starting composition and grain size as the Skagerrak sandstone reservoirs and B) the HPHT Skagerrak sandstones from the Egret, Heron and Skua fields.

Tables:

Table 1 – Present-day formation tops (Skagerrak Formation and Judy Member), formation pressure, temperature of the Egret, Heron and Skua fields.

Table 2 - Lithology thickness and type of the modelled layers for the Egret, Heron, Skua fields, with Sh: Shale, Sst: Sandstone, Non-Res.: Non-Reservoir Chalk and Res. Sst.: Reservoir Sandstone (80% Sand, 10% Silt and 10% Clay).

Table 3 - Non-reservoir North Sea chalk model parameters after Mallon and Swarbrick (2002 & 2008)

Table 4 - Homogenization temperatures of aqueous (Aqueous) and non-aqueous (Non) fluid inclusions in quartz overgrowth, feldspar and carbonate cements

Table 5 –Fe/Mg-ratio from SEM-EDS measurements of chlorite coats of the Egret, Heron and Skua samples

Table 6 - Calculated, temperature dependent quartz precipitation rates, with T for temperature, r for precipitation rate, gl for linear outgrowth rate and tc for critical time to enclose a fluid inclusion of 4 µm.

References

Aase, N.E., Bjorkum, P.A., Nadeau, P.H., 1996. The effect of grain-coating microquartz on preservation of reservoir porosity. AAPG Bulletin 80, 1654-1673.

Ajdukiewicz, J.M., Lander, R.H., 2010. Sandstone reservoir quality prediction: The state of the art. AAPG Bulletin 94, 1083-1091.

Aase, N.E., Walderhaug, O., 2005. The effect of hydrocarbons on quartz cementation: diagenesis in the Upper Jurassic sandstones of the Miller Field, North Sea, revisited. Petroleum Geoscience 11, 215-223.

Ajdukiewicz, J.M., Larese, R.E., 2012. How clay grain coats inhibit quartz cement and preserve porosity in deeply buried sandstones: Observations and experiments. AAPG Bulletin 96, 2091-2119.

Allen, P.A., Allen, J.R., 1990. Basin analysis: principles and applications. Blackwell scientific publications.

Andrews-Speed, C., Oxburgh, E.R., Cooper, B., 1984. Temperatures and depth-dependent heat flow in western North Sea. AAPG Bulletin 68, 1764-1781.

Anjos, S., De Ros, L., Silva, C., 2003. Chlorite authigenesis and porosity preservation in the Upper Cretaceous marine sandstones of the Santos Basin, offshore eastern Brazil: International Association of Sedimentology Special Publication 34. Clay Mineral Cements in Sandstones. International Association of Sedimentologists, Special Publication 34, 291-316.

Beard, D., Weyl, P., 1973. Influence of Texture on Porosity and Permeability of Unconsolidated Sand. AAPG Bulletin 57, 349-369.

Becker, S., Eichhubl, P., Laubach, S., Reed, R., Lander, R., Bodnar, R., 2010. A 48 my history of fracture opening, temperature, and fluid pressure: Cretaceous Travis Peak Formation, East Texas basin. Geological Society of America Bulletin 122, 1081-1093.

Bishop, D.J., 1996. Regional distribution and geometry of salt diapirs and supra-Zechstein Group faults in the western and central North Sea. Marine and petroleum geology 13, 355-364.

Bjorkum, P.A., Walderhaug, O., Aase, N.E., 1993. A model for the effect of illitization on porosity and quartz cementation of sandstones. Journal of Sedimentary Research 63.

Bjorkum, P.A. 1996. How important is pressure in causing dissolution of quartz in sandstones? Journal; of Sedimentary Research 66, 147-154

Bjorlykke, K., 2014. Relationships between depositional environments, burial history and rock properties. Some principal aspects of diagenetic process in sedimentary basins. Sedimentary Geology 301, 1-14.

Bjørlykke, K., 1999. An overview of factors controlling rates of compaction, fluid generation and flow in sedimentary basins, Growth, Dissolution and Pattern Formation in Geosystems. Springer, pp. 381-404.

Bloch, S., Lander, R.H., Bonnell, L., 2002. Anomalously high porosity and permeability in deeply buried sandstone reservoirs: Origin and predictability. AAPG Bulletin 86, 301-328.

De Jong, M., Smith, D., Nio, S., Hardy, N., 2006. Subsurface correlation of the Triassic of the UK southern Central Graben: new look at an old problem. First Break 24.

di Primio, R., Neumann, V., 2008. HPHT reservoir evolution: a case study from Jade and Judy fields, Central Graben, UK North Sea. International Journal of Earth Sciences 97, 1101-1114.

Downey, P. J., Hodgseon, D. M., Worden, R. H., 2011. Pre-requisites, processes, and prediction of chlorite grain coatings in petroleum reservoirs: A revies of subsurface examples. Marine and Petroleum Geology 32,63-75, doi:10.1016/j.marpetgeo.2011.11.007.

Ehrenberg, S., 1993. Preservation of anomalously high porosity in deeply buried sandstones by grain-coating chlorite: examples from the Norwegian continental shelf. AAPG Bulletin 77, 1260-1286.

Ehrenberg, S., Nadeau, P., Steen, Ø., 2008. A megascale view of reservoir quality in producing sandstones from the offshore Gulf of Mexico. AAPG Bulletin 92, 145-164.

Erratt, D., Thomas, G., Wall, G., 1999. The evolution of the central North Sea Rift, Petroleum Geology of Northwest Europe: Proceedings of the 5th Conference. Geological Society, London, pp. 63-82.

French, M.W., Worden, R.H., 2013. Orientation of microcrystalline quartz in the Fontainebleau Formation, Paris Basin and why it preserves porosity. Sedimentary Geology.

French, M.W., Worden, R.H., Mariani, E., Larese, R.E., Mueller, R.R., Kliewer, C.E., 2012. Microcrystalline Quartz Generation and the Preservation of Porosity In Sandstones: Evidence from the Upper Cretaceous of the Subhercynian Basin, Germany. Journal of Sedimentary Research 82, 422-434.

Glennie, K.W., 1998. Petroleum geology of the North Sea: basic concepts and recent advances. Blackwell Publishing.

Goldsmith, P., Hudson, G., Van Veen, P., 2003. Triassic. The Millenium Atlas: Petroleum geology of the central and northern North Sea: Geological Society (London) 105.

Goldsmith, P., Rich, B., Standring, J., 1995. Triassic correlation and stratigraphy in the south Central Graben, UK North Sea. Geological Society, London, Special Publications 91, 123-143.

Goldstein, R.H., Reynolds, T.J., 1994. Systematics of fluid inclusions in diagenetic minerals: SEPM Short Course 31. Society for Sedimentary Geology, 199.

Gowers, M.B., Sæbøe, A., 1985. On the structural evolution of the Central Trough in the Norwegian and Danish sectors of the North Sea. Marine and Petroleum Geology 2, 298-318.

Grant, N.T., Middleton, A.J., Archer, S., 2014. Porosity trends in the Skagerrak Formation, Central Graben, United Kingdom Continental Shelf: The role of compaction and pore pressure history. AAPG Bulletin 98, 1111-1143.

Grigsby, J.D., 2001. Origin and growth mechanism of authigenic chlorite in sandstones of the lower Vicksburg Formation, south Texas. Journal of Sedimentary Research 71, 27-36.

Grove, C., Jerram, D.A., 2011. jPOR: An ImageJ macro to quantify total optical porosity from blue-stained thin sections. Computers & Geosciences 37, 1850-1859.

Guven, N., Hower, W.F., Davies, D.K., 1980. Nature of authigenic illites in sandstone reservoirs. Journal of Sedimentary Research 50.

Haile, B.G., Hellevang, H., Aagaard, P., Jahren, J., 2015. Experimental nucleation and growth of smectite and chlorite coatings on clean feldspar and quartz grain surfaces. Marine and Petroleum Geology.

Heald, M., Larese, R., 1974. Influence of coatings on quartz cementation. Journal of Sedimentary Research 44, 1269-1274.

Hillier, S., Velde, B., 1992. Chlorite interstratified with a 7 mineral: an example from offshore Norway and possible implications for the interpretation of the composition of diagenetic chlorites. Clay Minerals 27, 475-475.

Hillier, S., 1994. Pore-lining chlorites in siliciclastic reservoir sandstones: electron microprobe, SEM and XRD data, and implications for their origin. Clay Minerals 29, 665-680.

Humphreys, B., Kemp, S. J., Lott, G. K., Dharmayanti, D. A., Samsori, I., 1994. Origin of grain-coating chlorite by smectite transformation; an example from Miocene sandstones, North Sumatra back-arc basin, Indonesia. Clay Minerals 29, 681-692.

Houseknecht, D.W., 1988. Intergranular pressure solution in four quartzose sandstones. Journal of Sedimentary Research 58.

Isaksen, G.H., 2004. Central North Sea hydrocarbon systems: Generation, migration, entrapment, and thermal degradation of oil and gas. AAPG Bulletin 88, 1545-1572.

Kape, S., De Souza, O.D., Bushnaq, I., Hayes, M., Turner, I., 2010. Predicting production behaviour from deep HPHT Triassic reservoirs and the impact of sedimentary architecture on recovery, Geological Society, London, Petroleum Geology Conference series. Geological Society of London, pp. 405-417.

Lander, R.H., Larese, R.E., Bonnell, L.M., 2008. Towards more accurate quartz cement models: The importance of euhedral versus noneuhedral growth rates. AAPG Bulletin 92, 1537-1563.

Lundegard, P.D., 1992. Sandstone porosity loss; a" big picture" view of the importance of compaction. Journal of Sedimentary Petrology 62, 250-260.

Maast, T.E., Jahren, J., Bjørlykke, K., 2011. Diagenetic controls on reservoir quality in Middle to Upper Jurassic sandstones in the South Viking Graben, North Sea. AAPG Bulletin 95, 1883-1905.

Mallon, A., Swarbrick, R., 2002. A compaction trend for non-reservoir North Sea Chalk. Marine and Petroleum Geology 19, 527-539.

Mallon, A.J., Swarbrick, R.E., Katsube, T.J., 2005. Permeability of fine-grained rocks: New evidence from chalks. Geology 33, 21-24.

Matlack, K. S., D. W. Houseknecht, and K. R. Applin, 1989. Emplacement of clay into sand by infiltration. Journal of Sedimentary Petrology, 59, p. 77–87.

Marchand, A.M.E., Smalley, P.C., Haszeldine, R.S., Fallick, A.E., 2002. Note on the importance of hydrocarbon fill for reservoir quality prediction in sandstones. AAPG Bulletin 86, 1561-1571.

Matthews, W.J., Hampson, G.J., Trudgill, B.D., Underhill, J.R., 2007. Controls on fluviolacustrine reservoir distribution and architecture in passive salt-diapir provinces: Insights from outcrop analogs. AAPG Bulletin 91, 1367-1403.

McBride, E.F., 1989. Quartz cement in sandstones: a review. Earth-Science Reviews 26, 69-112.

McKie, T., 2011. Architecture and behavior of dryland fluvial reservoirs, Triassic Skagerrak Formation, central North Sea, in: Davidson, S.K., Leleu, S., North, C.P. (Eds.), SEPM Special Publication, p. 26.

McKie, T., Audretsch, P., 2005. Depositional and structural controls on Triassic reservoir performance in the Heron Cluster, ETAP, Central North Sea, Geological Society, London, Petroleum Geology Conference series. Geological Society of London, pp. 285-297.

McKie, T., Jolley, S., Kristensen, M., 2010. Stratigraphic and structural compartmentalization of dryland fluvial reservoirs: Triassic Heron Cluster, Central North Sea. Geological Society, London, Special Publications 347, 165-198.

Molenaar, N., Cyziene, J., Sliaupa, S., Craven, J., 2008. Lack of inhibiting effect of oil emplacement on quartz cementation: Evidence from Cambrian reservoir sandstones, Paleozoic Baltic Basin. Geological Society of America Bulletin 120, 1280-1295.

Munz, I., Johansen, H., Johansen, I., 1999. Characterisation of composition and PVT properties of petroleum inclusions: Implications of reservoir filling and compartmentalisation, SPE Annual Technical Conference and Exhibition. Society of Petroleum Engineers.

Munz, I.A., 2001. Petroleum inclusions in sedimentary basins: systematics, analytical methods and applications. Lithos 55, 195-212.

Nguyen, B.T.T., Jones, S.J., Goulty, N.R., Middleton, A.J., Grant, N., Ferguson, A., Bowen, L., 2013. The role of fluid pressure and diagenetic cements for porosity preservation in Triassic fluvial reservoirs of the Central Graben, North Sea. AAPG Bulletin 97, 1273-1302.

Oakes, C.S., Bodnar, R.J., Simonson, J.M., 1990. The system NaCl-CaCl2-H2O I. The ice liquidus at 1 atm total pressure. Geochimica et Cosmochimica Acta 54, 603-610.

Osborne, M.J., Swarbrick, R.E., 1997. Mechanisms for generating overpressure in sedimentary basins: A reevaluation. AAPG Bulletin 81, 1023-1041.

Osborne, M.J., Swarbrick, R.E., 1999. Diagenesis in North Sea HPHT clastic reservoirs—Consequences for porosity and overpressure prediction. Marine and Petroleum Geology 16, 337-353.

Parsons, I., Thompson, P., Lee, M.R., Cayzer, N., 2005. Alkali feldspar microtextures as provenance indicators in siliciclastic rocks and their role in feldspar dissolution during transport and diagenesis. Journal of Sedimentary Research 75, 921-942.

Paxton, S., Szabo, J., Ajdukiewicz, J., Klimentidis, R., 2002. Construction of an intergranular volume compaction curve for evaluating and predicting compaction and porosity loss in rigid-grain sandstone reservoirs. AAPG Bulletin 86, 2047-2067.

Pittman, E.D., Larese, R.E., Heald, M.T., 1992. Clay coats: occurrence and relevance to preservation of porosity in sandstones. Pittman, eds., Origin, diagenesis, and petrophysics of clay minerals in sandstones: SEPM Special Publication 47, 241-255.

Pittman, E.D., Lumsden, D.N., 1968. Relationship Between Chlorite Coatings on Quartz Grains and Porosity, Spiro Sand, Oklahoma: NOTES. Journal of Sedimentary Petrology 38.

Ramm, M., and K. Bjørlykke, 1994, Porosity/depth trends in reservoir sandstones: Assessing the quantitative effects of varying pore pressure, temperature history and mineral- ogy, Norwegian shelf area: Clay Minerals, v. 29, p. 475– 490, doi:10.1180/claymin.1994.029.4.07.

Saigal, G.C., Bjørlykke, K., Larter, S., 1992. The Effects of Oil Emplacement on Diagenetic Processes: Examples from the Fulmar Reservoir Sandstones, Central North Sea: Geologic Note (1). AAPG Bulletin 76, 1024-1033.

Sathar, S., Worden, R.H., Faulkner, D.R., Smalley, P.C., 2012. The Effect of Oil Saturation On the Mechanism of Compaction In Granular Materials: Higher Oil Saturations Lead To More Grain Fracturing and Less Pressure Solution. Journal of Sedimentary Research 82, 571-584.

Sathar, S and Jones, S.J. 2016. Fluid overpressure as a control on sandstone reservoir quality in a mechanical compaction dominated setting: Magnolia Field, Gulf of Mexico. Terra Nova, In Press.

Schneider, F., and S. Hay, 2001, Compaction model for quartzose sandstones application to the Garn Formation, Haltenbanken, mid-Norwegian continental shelf: Marine and Petroleum Geology, v. 18, p. 833–848, doi:10.1016 /S0264-8172(01)00032-0.

Sheldon, H.A., Wheeler, J., Worden, R.H., Cheadle, M.J., 2003. An analysis of the roles of stress, temperature, and pH in chemical compaction of sandstones. Journal of Sedimentary Research 73, 64-71.

Smith, R., Hodgson, N., Fulton, M., 1993. Salt control on Triassic reservoir distribution, UKCS central North Sea, Geological Society, London, Petroleum Geology Conference series. Geological Society of London, pp. 547-557.

Storvoll, V., Bjørlykke, K., Karlsen, D., Saigal, G., 2002. Porosity preservation in reservoir sandstones due to grain-coating illite: a study of the Jurassic Garn Formation from the Kristin and Lavrans fields, offshore Mid-Norway. Marine and Petroleum Geology 19, 767-781.

Swarbrick, R., Osborne, M., Grunberger, D., Yardley, G., Macleod, G., Aplin, A., Larter, S., Knight, I., Auld, H., 2000. Integrated study of the Judy field (Block 30/7a)—An overpressured central North Sea oil/gas field. Marine and Petroleum Geology 17, 993-1010.

Taylor, T.R., Kittridge, M.G., Winefield, P., Bryndzia, L.T., Bonnell, L.M., 2015. Reservoir quality and rock properties modeling–Triassic and Jurassic sandstones, greater Shearwater area, UK Central North Sea. Marine and Petroleum Geology 65, 1-21.

Vagle, G.B., Hurst, A., Dypvik, H., 1994. Origin of quartz cements in some sandstones from the Jurassic of the Inner Moray Firth (UK). Sedimentology 41, 363-377.

Walderhaug, O., 1990. A Fluid Inclusion Study of Quartz-Cemented Sandstones from Offshore Mid-Norway—Possible Evidence for Continued Quartz Cementation During Oil Emplacement. Journal of Sedimentary Research 60.

Walderhaug, O., 1994a. Precipitation rates for quartz cement in sandstones determined by fluid-inclusion microthermometry and temperature-history modeling. Journal of Sedimentary Research 64.

Walderhaug, O., 1994b. Temperatures of quartz cementation in Jurassic sandstones from the Norwegian continental shelf-evidence from fluid inclusions. Journal of Sedimentary Research 64.

Walderhaug, O., 1996. Konetic modeling of quartz cementation and porosity loss in deeply buried sandstoe reservoirs. AAPG Bulletin 80, 731-745.

Weibel, R., 1998. Diagenesis in oxidising and locally reducing conditions—an example from the Triassic Skagerrak Formation, Denmark. Sedimentary Geology 121, 259-276.

Wilson, M., Wilson, L., Patey, I., 2014. The influence of individual clay minerals on formation damage of reservoir sandstones: a critical review with some new insights. Clay Minerals 49, 147-164.

Wilson, M.D., Pittman, E.D., 1977. Authigenic clays in sandstones; recognition and influence on reservoir properties and paleoenvironmental analysis. Journal of Sedimentary Research 47, 3-31.

Worden, R.H., Oxtoby, N.H., Smalley, P.C., 1998. Can oil emplacement prevent quartz cementation in sandstones? Petroleum Geoscience 4, 129-137.

Worden, R., Morad, S., 2000. Quartz cementation in oilfield sandstones: a review of the key controversies. Special Publication, International Association of Sedimentologists, 1-20.

Worden, R., Morad, S., 2003. Clay minerals in sandstones: controls on formation, distribution and evolution. Wiley Online Library.

Worden, R.H., French, M.W., Mariani, E., 2012. Amorphous silica nanofilms result in growth of misoriented microcrystalline quartz cement maintaining porosity in deeply buried sandstones. Geology 40, 179-182.

Field		Egret	Heron	Skua
Well		22/24d-10	22/29-5RE	22/24b-7
Top Skagerrak Formation	[m TVDSS]	4310	4289	3557
Top Judy Member	[m TVDSS]	4368	4312	3557
Judy Member				
RFT Formation pressure	[MPa]	85.6 - 86.8	86.8	63.7 - 66.8
RFT Temperature	[°C]	175 - 183	176 - 178	160
Fluid inclusion sample	[m TVDSS]	4565	4412	3608
			4419	3615

Group/ Formation	Egret		Heron		Skua	
	Thick.	Lithology	Thick.	Lithology	Thick.	Lithology
	[m]	[-]	[m]	[-]	[m]	[-]
Water	91	Water	93	Water	97	Water
Nordland	1409	Shale	1407	Shale	1762	Shale
Lark/Horda	1341	Shale	1396	Shale	957	Shale
Tay	45	Shale	15	Sandy Sh.		
Balder	13	Shale	18	Shale	12	Shale
Sele	25	Sandy Sh.	31	Sandy Sh.	21	Shale
Forties	168	Sandstone	187	Sandstone	79	Sandstone
Lista	60	Silty Sh.	49	Silty Sh.		
Andrew			51	Siltstone	81	Siltstone
Maureen	142	Marl	82	Marl	54	Marl
Ekofisk	76	Chalk	94	Chalk	76	Marl
Tor	446	Chalk	459	Chalk	300	Chalk
Hod	293	Non-Res.	335	Non-Res.	98	Non-Res.
Herring	30	Chalk	9	Marl		
Hidra	10	Shale				
Valhall	92	Chalk	63	Marl	19	Marl
Kimeridge Clay	4	Shale	0	Shale	0	Shale
Heather	33	Shale	0	Shale	0	Shale
Pentland	33	Shale				
Joshua	0	Silty Shale	0	Silty Shale	0	Silty Sh.
Josephine	0	Res. Sst	0	Res. Sst	0	Res. Sst
Jonathan	0	Silty Sh.	0	Silty Sh.	0	Silty Sh.
Joanne	0	Res. Sst	23	Res. Sst	0	Res. Sst
Julius	58	Silty Sh.	41	Silty Sh.	0	Silty Sh.
Judy	302	Res. Sst	339	Res. Sst	468	Res. Sst
Smith Bank	230	Silty Sh.	200	Silty Sh.	118	Silty Sh.
Zechstein	200	Salt	208	Salt	207	Salt

Model Parameter (Hod Formation)			
Mechanical compaction		**Permeability**	
Porosity	**Depth**	**Porosity**	**Permeability**
[%]	**[m]**	**[%]**	**[log(mD)]**
70.00	0	70.00	1.00
18.00	1300	30.00	-1.00
12.50	2100	25.00	-3.00
8.00	3100	20.00	-5.50
5.00	4500	12.50	-7.20
		9.00	-7.20
		5.00	-7.20

	Egret		Heron				Skua			
FI Host	**Sample 1**		**Sample 1**		**Sample 2**		**Sample 1**		**Sample 2**	
	Aqueous [°C]	**Non** [°C]	**Aqueous** [°C]	**Non** [°C]	**Aqueous** [°C]	**Non** [°C]	**Aqueous** [°C]	**Non** [°C]	**Aqueous** [°C]	**Non** [°C]
Quartz OG	145.4		104.0	69.8	133.7		133.4		132.6	83.3
Quartz OG	146.0		106.0	72.1	141.5		135.8		133.1	
Quartz OG	147.9		111.0	75.3	143.1		135.9		133.3	
Quartz OG	149.0		116.0	76.1	143.6		137.1		133.5	
Quartz OG	149.4			76.3	144.4		137.3		136.1	
Quartz OG	150.2				145.4		137.3		137.3	
Quartz OG	150.2				162.2		139.3		138.6	
Quartz OG	150.7				163.3		139.9		139.9	
Quartz OG	151.6						140.4			
Quartz OG	152.2						140.8			
Quartz OG	152.3						140.8			
Quartz OG	153.4						141.5			
Quartz OG	154.4						142.3			
Quartz OG	155.0						143.0			
Quartz OG	155.8						144.0			
Quartz OG	160.1						144.2			
Quartz OG	166.5						144.6			
Quartz OG	166.6						145.7			
Quartz OG	171.0						146.8			
Quartz OG							154.5			
Quartz OG							156.2			
Feldspar	145.7			60.0		44.8		81.6		83.6
Feldspar	147.0			61.4		66.7		85.6		88.1
Feldspar	148.2			61.9		67.0		85.7		
Feldspar				62.3		70.8		87.9		
Feldspar				75.4		74.4		88.6		
Feldspar				75.5		75.4		88.7		
Feldspar				77.0		75.5		88.9		
Feldspar				77.3		75.8		91.0		
Feldspar				77.8		75.9		91.7		
Feldspar				78.9		76.4		100.1		
Feldspar				87.9		77.1		100.5		
Feldspar						81.4		118.2		
Carbonate									138.5	79.4
Carbonate									140.0	80.4
Carbonate									140.4	84.0
Carbonate									141.5	87.2
Carbonate									141.8	87.4
Carbonate									142.1	88.0
Carbonate									142.3	107.3
Carbonate									142.4	111.6
Carbonate									142.7	
Carbonate									143.4	
Carbonate									144.5	

Fe/Mg-ratio		
Egret	**Heron**	**Skua**
0.49	0.49	0.52
0.49	0.59	0.49
0.48	0.45	0.39
0.49	0.54	0.35
0.48	0.51	0.37
0.48	0.49	0.37
0.45	0.52	0.38
0.45	0.52	0.38
0.48	0.51	0.45
0.50	0.50	0.50
0.49	0.49	0.47
0.48	0.49	0.47
0.46	0.47	0.47
0.44	0.50	0.50
0.47	0.51	0.47
0.46	0.54	0.51
0.46	0.56	0.40
0.47	0.62	0.47
0.48	0.58	0.44
0.44	0.61	0.41
0.47	0.52	0.49
0.49	0.49	0.45
0.52	0.46	0.51
0.50	0.44	0.50
0.46	0.47	0.48
0.50	0.47	0.51
0.54	0.50	0.49
0.55	0.50	0.51
0.59	0.52	0.53
0.55	0.56	0.48
0.41	0.50	0.51
0.48	0.47	0.49
0.46		
0.47		
0.44		
0.46		
0.44		
0.42		
0.48	**0.51**	**0.46**

Temperature	**Precipitation rate [r]**	**Linear outgrowth [g_l]**		**Critical time [t_c] for 4µm**
[°C]	[mol/cm^2]	[cm/s]	[µm/Ma]	[Ma]
70	6.86539E-21	1.55661E-19	0.049089	81.48414
80	1.13937E-20	2.58333E-19	0.081468	49.09905
90	1.89089E-20	4.28726E-19	0.135203	29.5851
100	3.13809E-20	7.11509E-19	0.224381	17.82679
110	5.20793E-20	1.18081E-18	0.37238	10.7417
120	8.64301E-20	1.95966E-18	0.617998	6.472515
130	1.43438E-19	3.25222E-18	1.025621	3.900076
140	2.38048E-19	5.39735E-18	1.702107	2.350028
150	3.95062E-19	8.95737E-18	2.824795	1.416032
160	6.5564E-19	1.48655E-17	4.687993	0.853244
170	1.08809E-18	2.46706E-17	7.780131	0.51413

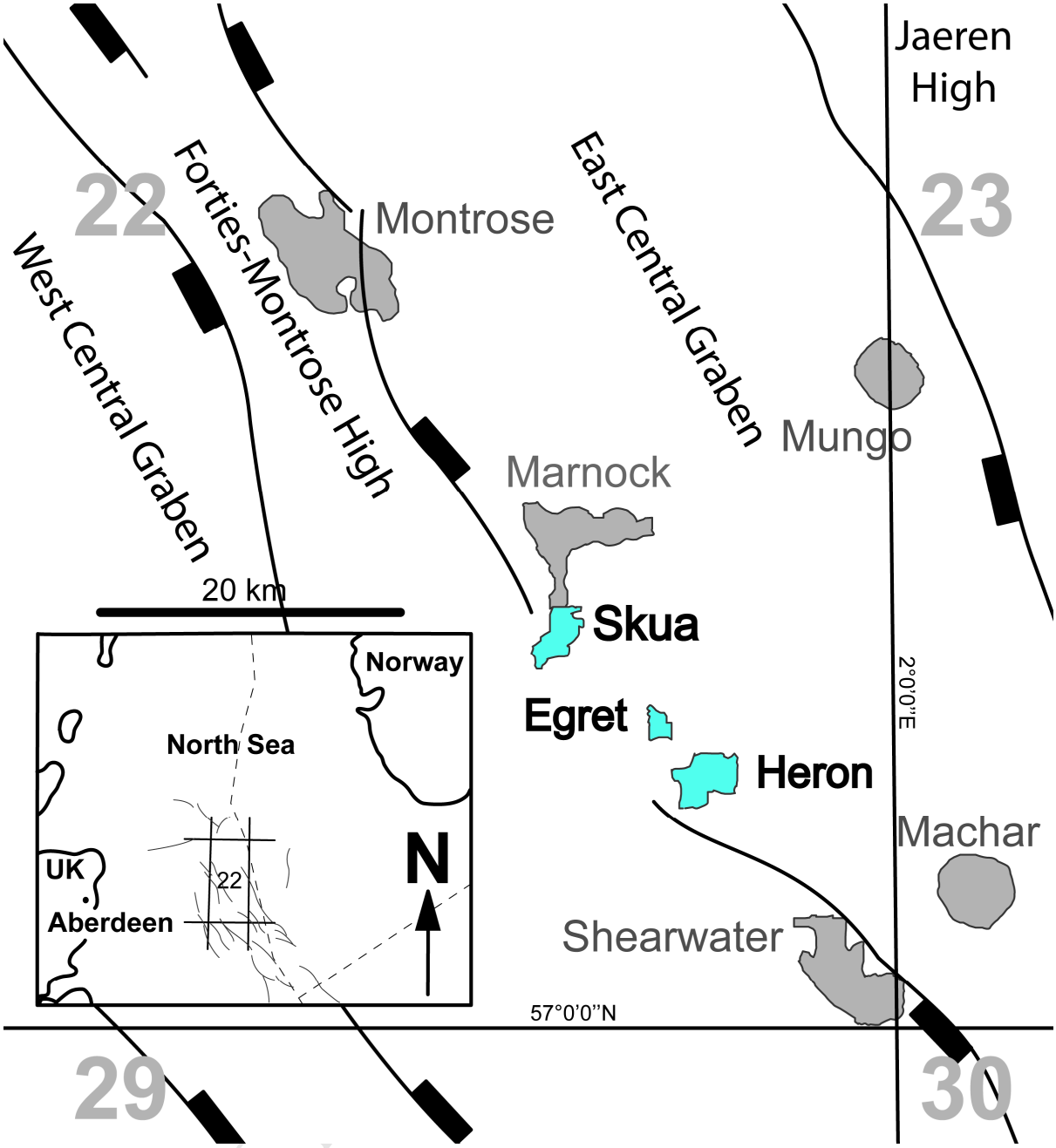
Jaeren
High
22
23
Fortries-Montrose High
East Central Graben
West Central Graben
Montrose
Mungo
Marnock
20 km
Skua
Norway
North Sea
Egret
Heron
2°0'0"E
Machar
UK
Aberdeen
22
N
Shearwater
57°0'0"N
29
30

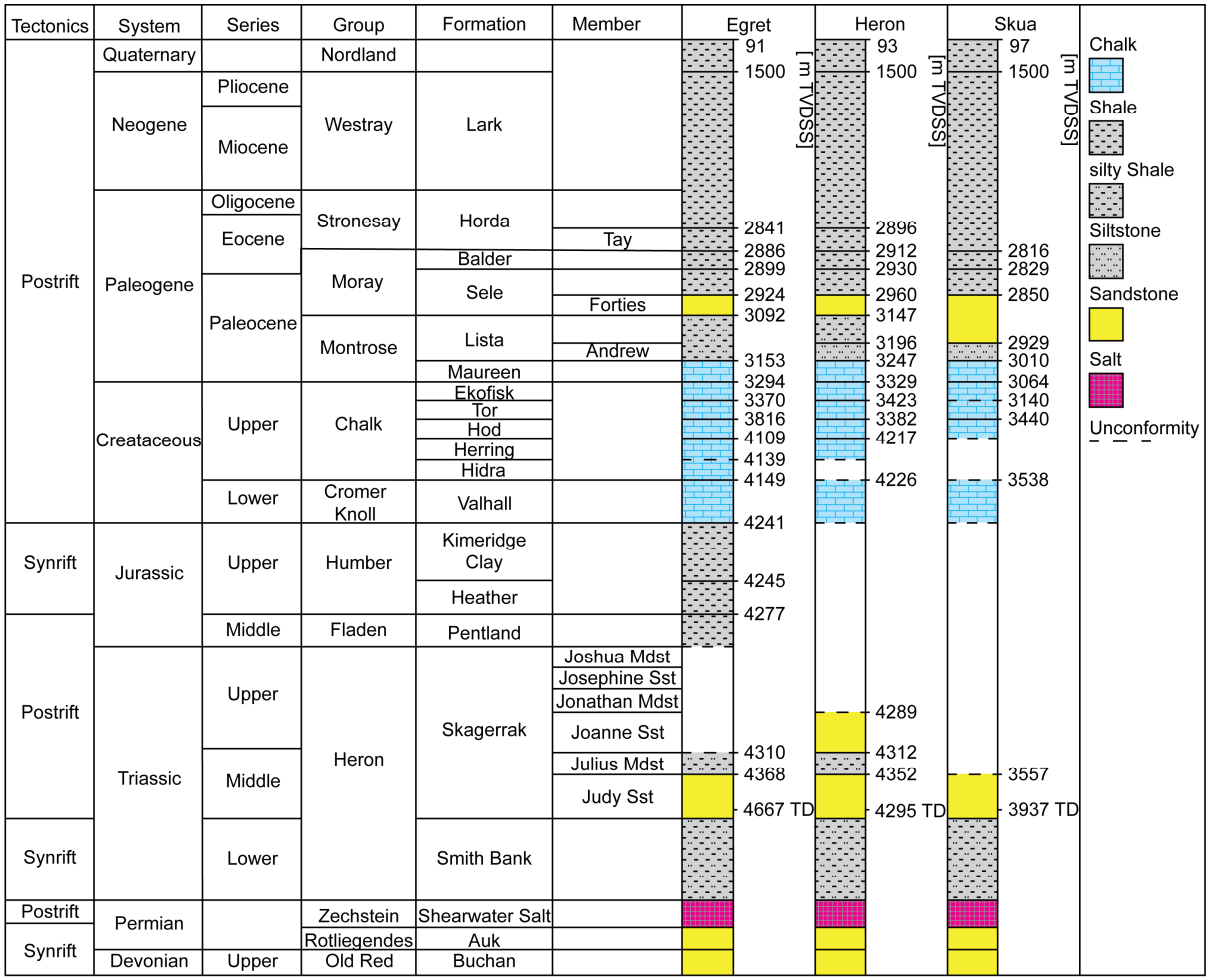

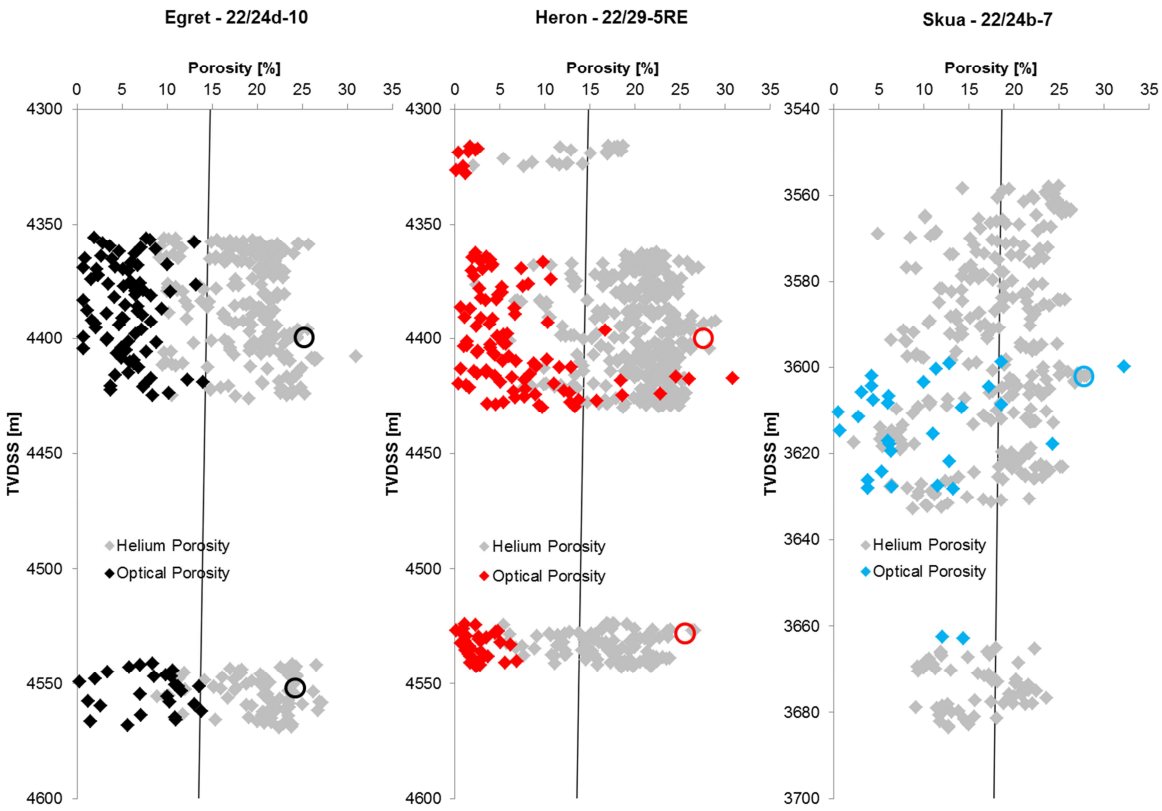

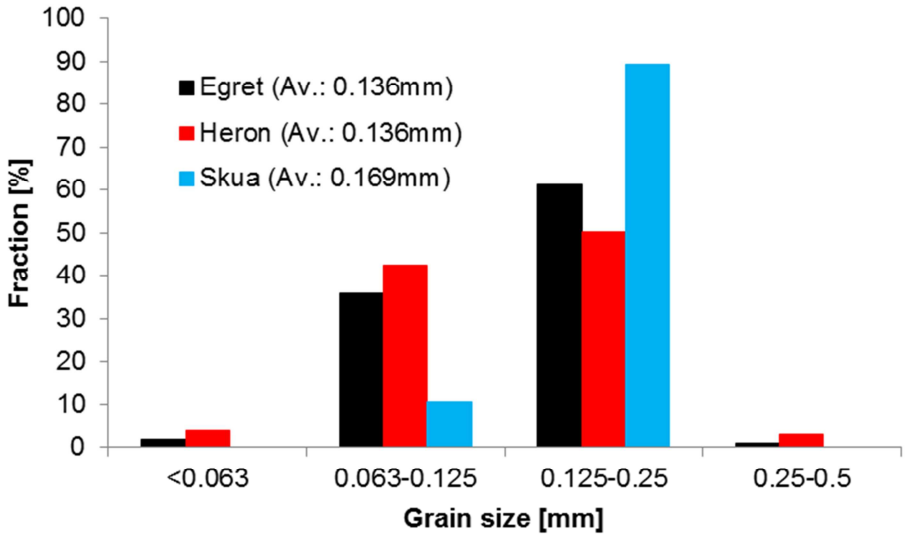

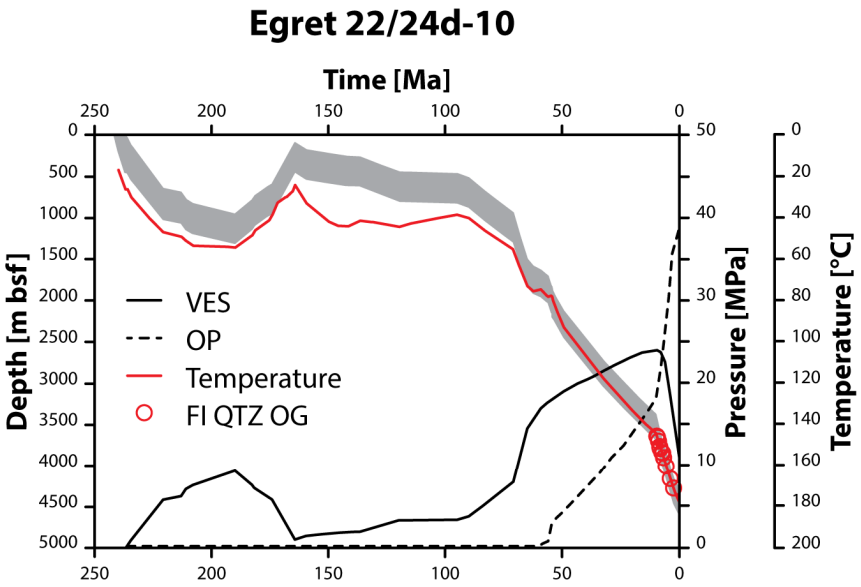
Egret 22/24d-10
Time [Ma]
Depth [m bsf]
Pressure [MPa]
Temperature [°C]
VES
OP
Temperature
FI QTZ OG

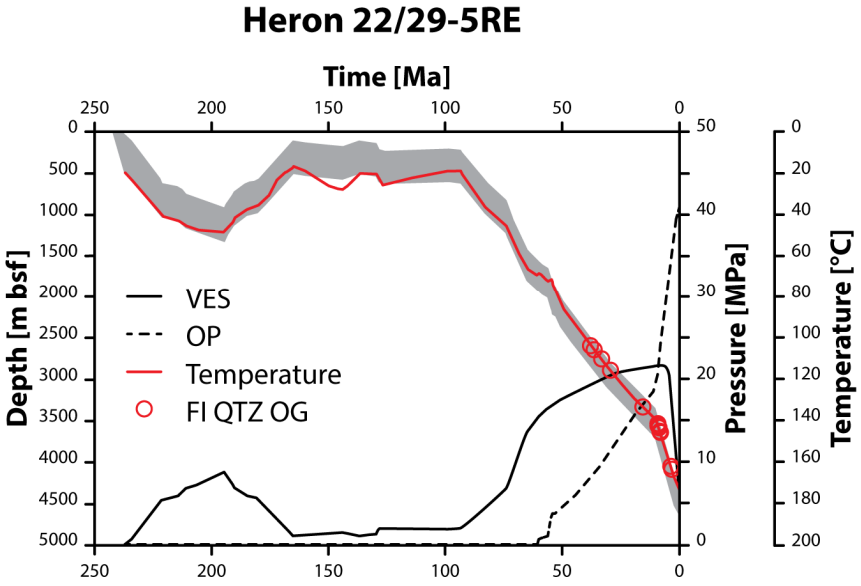
Heron 22/29-5RE
Time [Ma]
Depth [m bsf]
Pressure [MPa]
Temperature [°C]
VES
OP
Temperature
FI QTZ OG

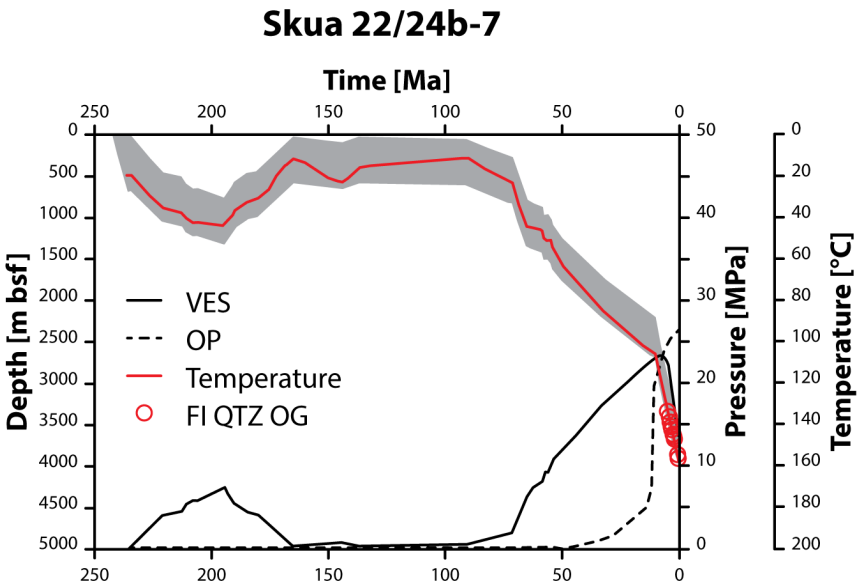
Skua 22/24b-7
Time [Ma]
Depth [m bsf]
Pressure [MPa]
Temperature [°C]
VES
OP
Temperature
FI QTZ OG

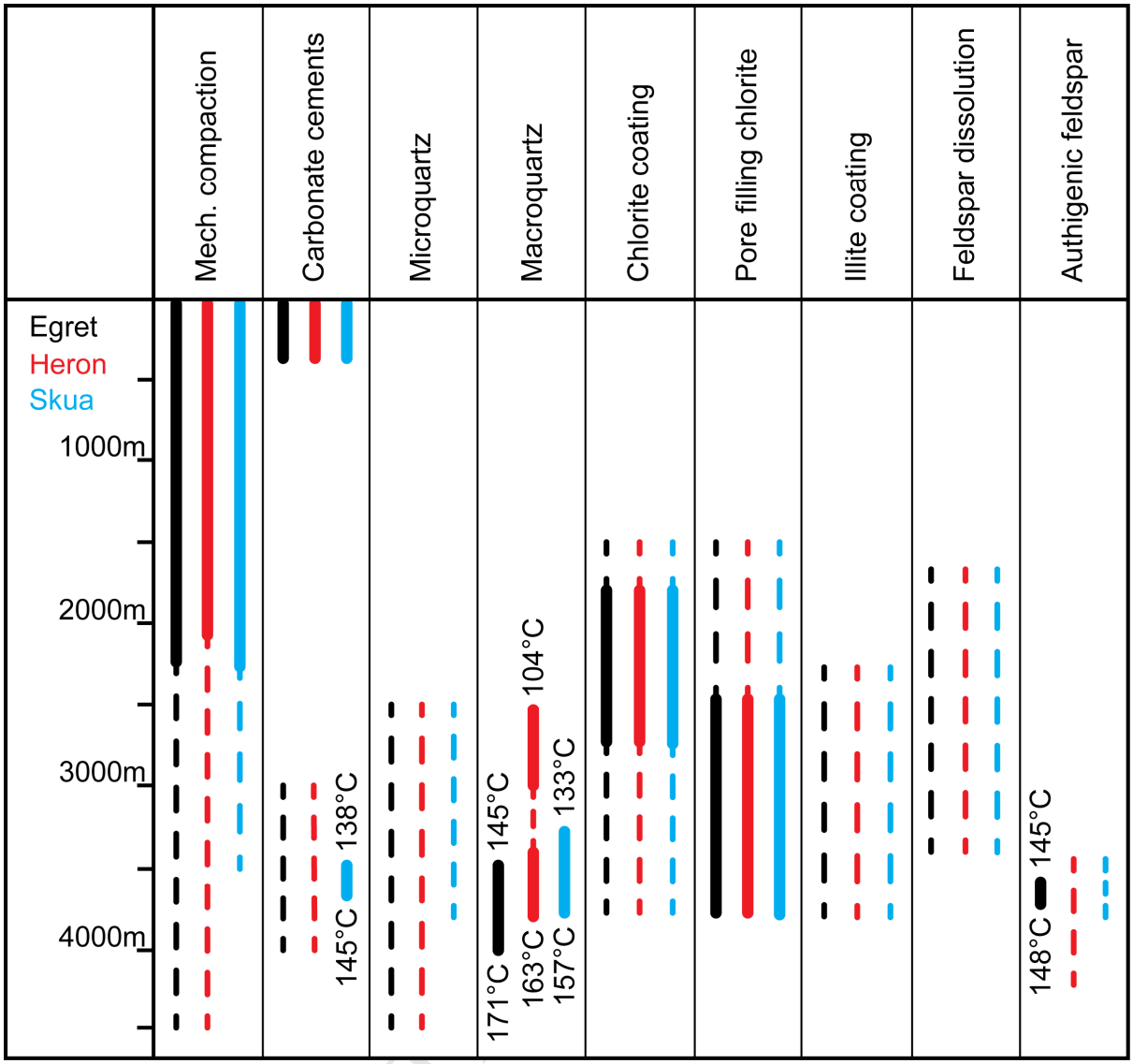

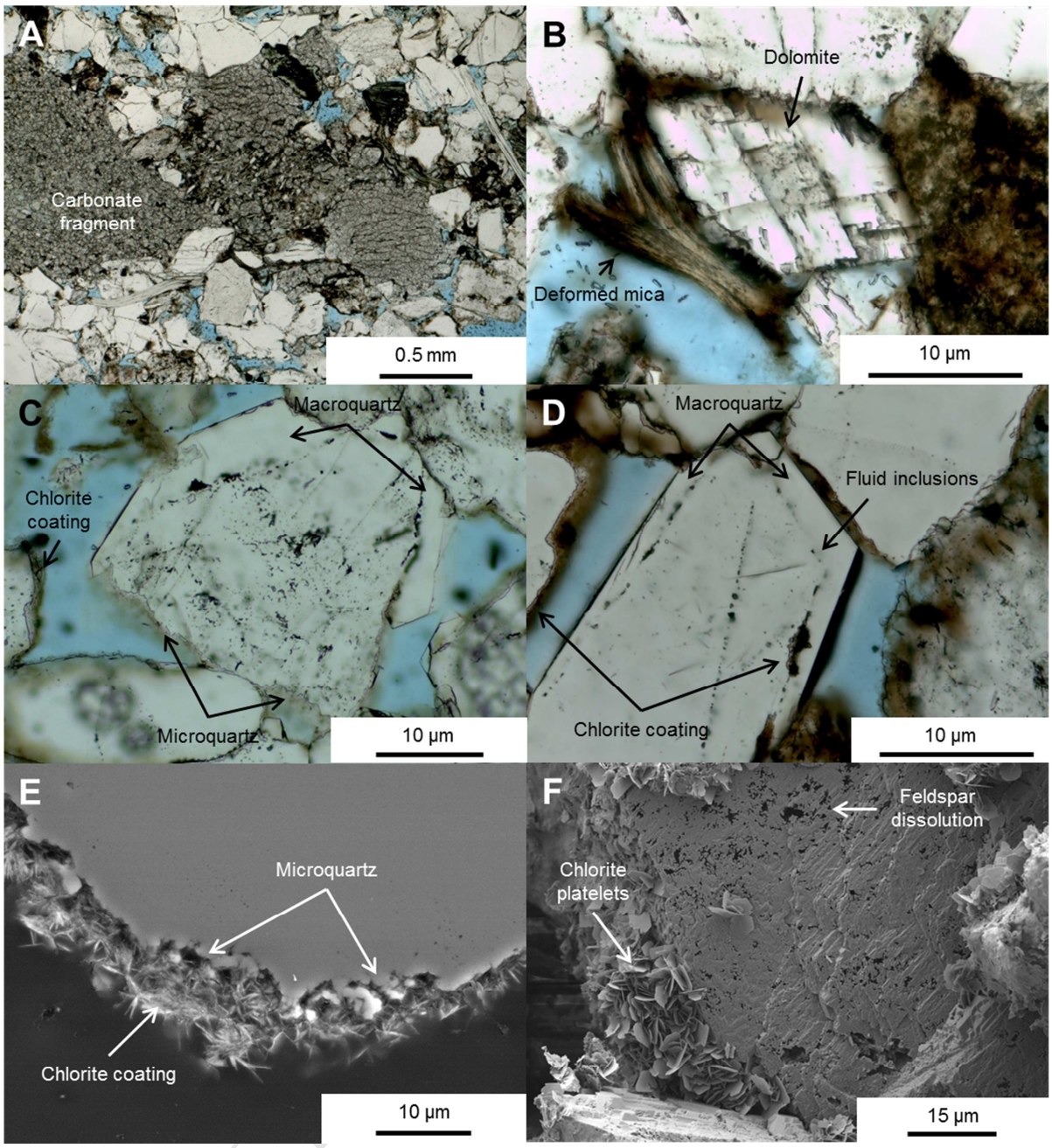
A
Carbonate fragment
0.5 mm
B
Dolomite
Deformed mica
10 µm
C
Macroquartz
Chlorite coating
Microquartz
10 µm
D
Macroquartz
Fluid inclusions
Chlorite coating
10 µm
E
Microquartz
Chlorite coating
10 µm
F
Feldspar dissolution
Chlorite platelets
15 µm

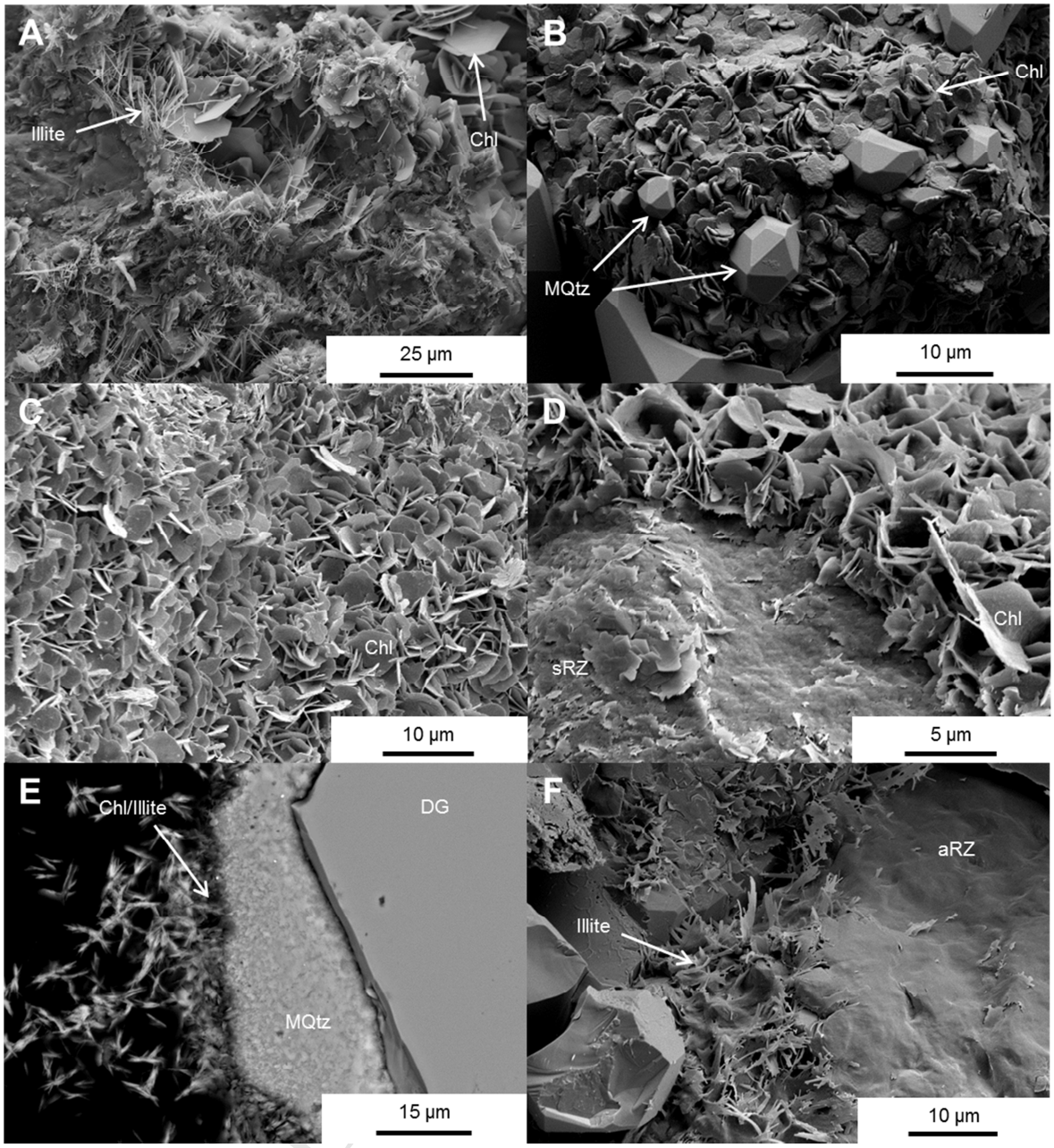
A
Illite
Chl
25 µm
B
Chl
MQtz
10 µm
C
Chl
10 µm
D
Chl
sRZ
5 µm
E
Chl/Illite
DG
MQtz
15 µm
F
aRZ
Illite
10 µm

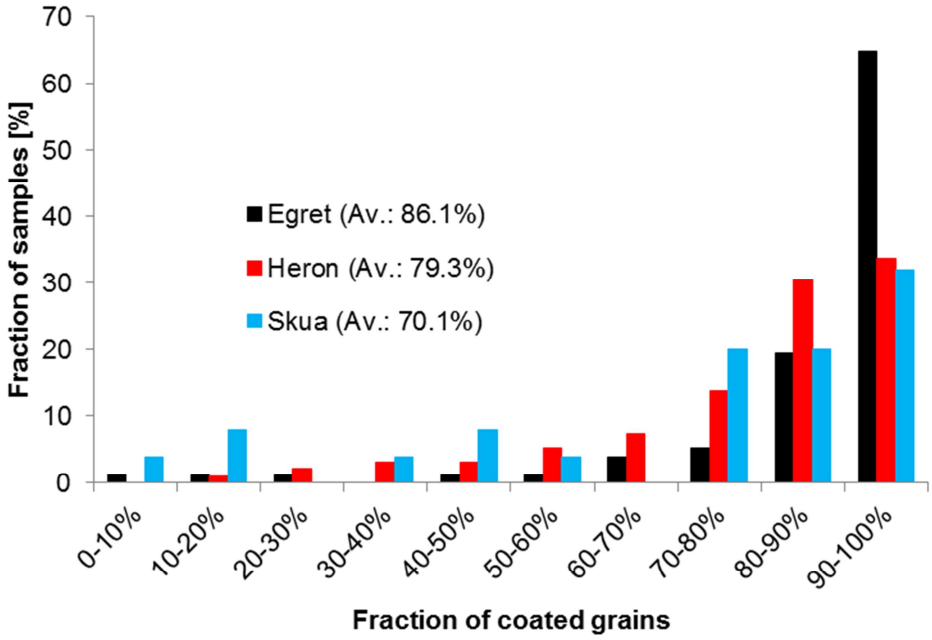

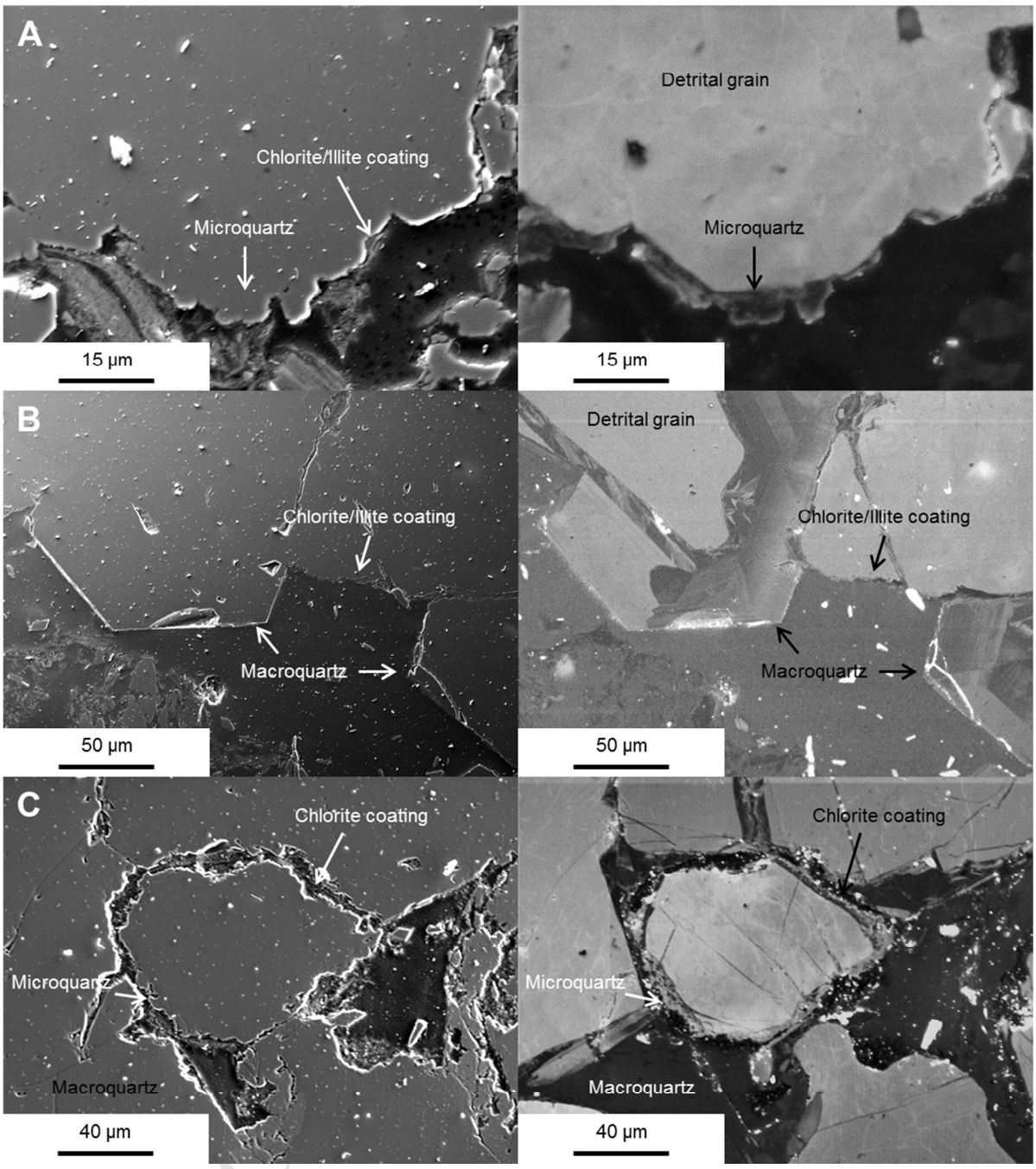
A
Chlorite/Illite coating
Microquartz
15 µm
Detrital grain
Microquartz
15 µm
B
Chlorite/Illite coating
Macroquartz
50 µm
Detrital grain
Chlorite/Illite coating
Macroquartz
50 µm
C
Chlorite coating
Microquartz
Macroquartz
40 µm
Chlorite coating
Microquartz
Macroquartz
40 µm

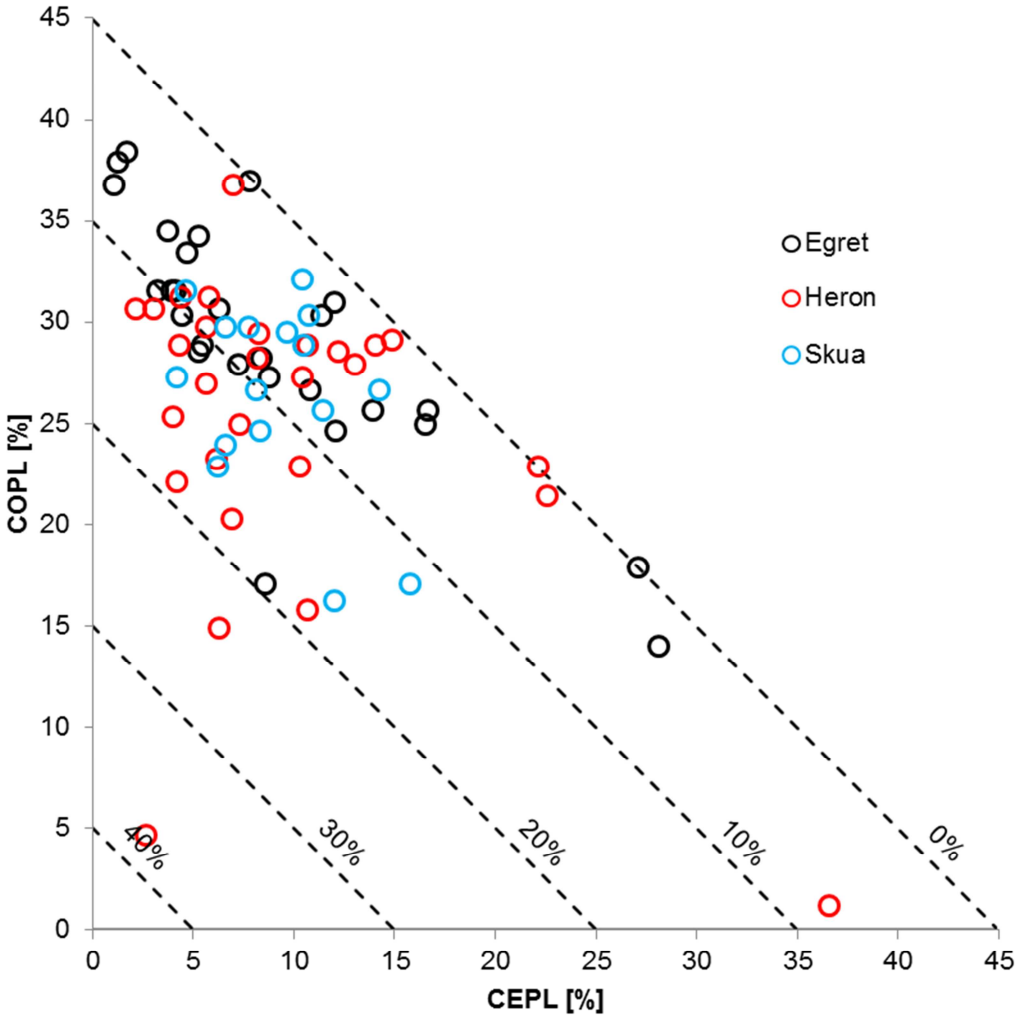

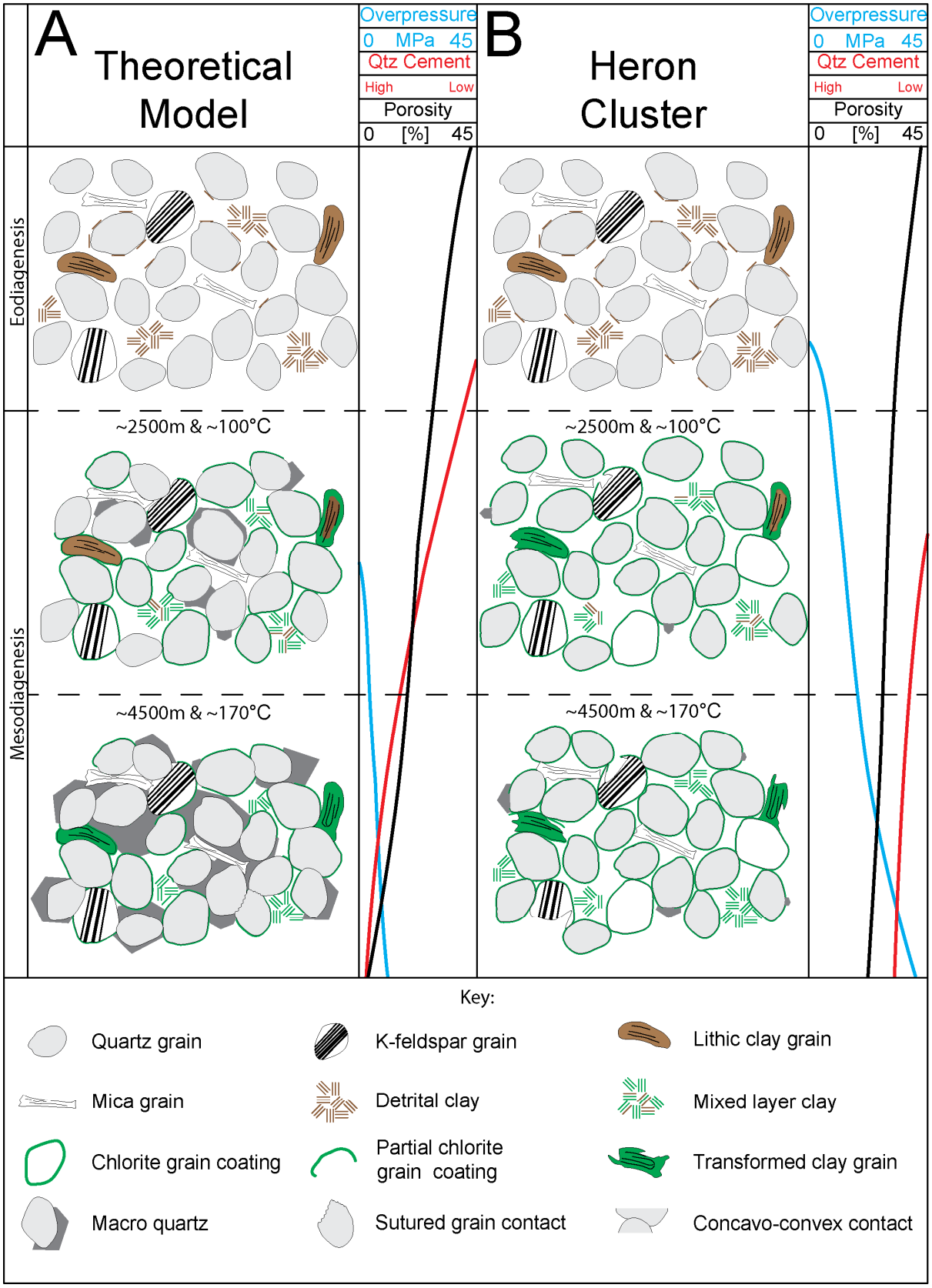
A
Theoretical Model
B
Heron Cluster
Overpressure
0 MPa 45
Qtz Cement
High Low
Porosity
0 [%] 45
Eodiagenesis
Mesodiagenesis
~2500m & ~100°C
~4500m & ~170°C
Key:
Quartz grain
K-feldspar grain
Lithic clay grain
Mica grain
Detrital clay
Mixed layer clay
Chlorite grain coating
Partial chlorite grain coating
Transformed clay grain
Macro quartz
Sutured grain contact
Concavo-convex contact